HIGH-TEMPERATURE SENSORS FOR ARMY GAS TURBINE ENGINES

B. G. Buehler, et al

Solar Division of International Harvester Company

Prepared for:

Army Air Mobility Research and Development Laboratory

November 1974

Unclassified

SECURITY CLASSIFICATION OF THIS PAGE (When Data Entered)

REPORT DOCUMENTATION PAGE	READ INSTRUCTIONS BEFORE COMPLETING FORM
1. REPORT NUMBER: USAAMRDL-TR-74-94	2. GOVT ACCESSION NO.
	3. RECIPIENT'S CATALOG NUMBER: AD/A-003 166
4. TITLE (and Subtitle): HIGH-TEMPERATURE SENSORS FOR ARMY GAS TURBINE ENGINES	5. TYPE OF REPORT & PERIOD COVERED: Final Report, June 1973 to August 1974
	6. PERFORMING ORG. REPORT NUMBER: RDR-1780-2
7. AUTHOR(s): B. G. Buehler, D. A. Rohy, W. A. Compton	8. CONTRACT OR GRANT NUMBER(s): DAAJ02-73-C-0085
9. PERFORMING ORGANIZATION NAME AND ADDRESS: Solar Division of International Harvester Company, 2200 Pacific Highway, San Diego, CA 92138	10. PROGRAM ELEMENT, PROJECT, TASK AREA & WORK UNIT NUMBERS: 1G162204AA7102
11. CONTROLLING OFFICE NAME AND ADDRESS: Eustis Directorate, U. S. Army Air Mobility R&D Laboratory, Fort Eustis, Va 23604	12. REPORT DATE: November 1974
	13. NUMBER OF PAGES: 61
14. MONITORING AGENCY NAME & ADDRESS (if different from Controlling Office)	15. SECURITY CLASS. (of this report): Unclassified
	15a. DECLASSIFICATION/DOWNGRADING SCHEDULE

16. DISTRIBUTION STATEMENT (of this Report)

Approved for public release; distribution unlimited.

17. DISTRIBUTION STATEMENT (of the abstract entered in Block 20, if different from Report)

18. SUPPLEMENTARY NOTES

19. KEY WORDS (Continue on reverse side if necessary and identify by block number)

Gas Turbines
Instruments
Pyrometers
Temperature Measurement

20. ABSTRACT (Continue on reverse side if necessary and identify by block number)

The turbine blade temperature measuring system views the rotating turbine blades of a gas turbine engine, and by measuring the emitted, infrared radiation, it produces a processed signal directly proportional to the temperature of the blades.

PRICES SUBJECT TO CHANGE

DD FORM 1 JAN 73 1473 EDITION OF 1 NOV 65 IS OBSOLETE

Unclassified

SECURITY CLASSIFICATION OF THIS PAGE (When Data Entered)

Initially, infrared energy is gathered by an optical sensor head positioned and targeted through the turbine case. The energy is focused on an armored fiber-optic bundle and conducted approximately 3 feet away. The bundle terminates into a photovoltaic diode which converts radiant energy into electric current. As the current generated is in the nanoampere region, amplification is required. A high-gain, low-drift amplifier is used in a current-to-voltage mode to provide a usable signal level for processing. The configuration described exists for a number of reasons. It allows electronics to be placed away from a hot engine; it allows early amplification of low signal levels to minimize electrical noise problems; and it places the major critical portion of the electronics in a less demanding environment.

The electrical signal from the preamp/detector is routed to the control unit. The signal is amplified by a gain stage which is variable to account for differences between sensor heads. After amplification, the signal is applied to a peak detector in the average peak and maximum peak modes. In the average mode, the composite signal is passed directly. The average peak and maximum peak mode circuits capture the peaks of the AC portion of the signal. The average mode is representative of the DC portion of the signal. After mode selection, the signal is fed to a linearizer. The nature of the signal is nonlinear, and the linearizer, as its name implies, provides a linear output and sets the system scale factor. A four-digit meter displays temperature on a scale of 1mV = 1° F. Laboratory accuracy is ±10° F from 1300° to 2100° F. Blade passing frequency cutoff occurs at 54 kHz (-3 dB).

Adapting a unique probe assembly to the Titan engine represents Solar's first application to a radial engine. The program demonstrated the feasibility of radiation pyrometry to Army gas turbine engines. Pyrometers are applicable to axial and radial engines.

PREFACE

This report, prepared by the Solar Division of International Harvester Company, describes the laboratory development of three high-temperature sensors and electronic signal processor for Army gas turbine engines.

The program was sponsored by the U.S. Army Air Mobility Research and Development Laboratory under Contract DAAJ02-73-C-0085 (DA Task 1G162204AA7102). The contracting officer's technical representative for the program was Mr. David Cale. The Solar Program Manager was Mr. W. A. Compton, Assistant Director of Research; and the principal investigator was Mr. B. G. Buehler, Research Engineer.

Special acknowledgment is extended to staff members of the Solar Research Laboratories. Engine entry analysis and probe designs were contributed by Mr. D. Timan, Senior Research Technician; design review and improvement suggestions were contributed by Mr. B. Nahid; and administrative and optical design assistance was provided by Dr. David A. Rohy.

TABLE OF CONTENTS

TABLE OF CONTENTS (Cont)

LIST OF ILLUSTRATIONS

LIST OF ILLUSTRATIONS (Cont)

LIST OF TABLES

INTRODUCTION

PROGRAM OBJECTIVE

The primary purpose of this task was to demonstrate the feasibility of radiation pyrometry application to Army gas turbine engines. Emphasis was placed on designing, assembling and testing a laboratory instrument radiation pyrometer system and attaining system performance improvements.

Secondary outputs from the program were an electronic simulator to ease measurement of system frequency response and preliminary digital system designs to increase system accuracy.

IMPORTANCE OF TURBINE BLADE TEMPERATURE MEASUREMENT

Increased gas turbine inlet temperatures combined with higher pressure ratios offer the greatest potential for improvements in the performance of advanced engines. Presently, experimental engines operating well above 2000° F are demonstrating that tremendous performance improvements are possible. At these very high inlet temperatures, the key parameter required (turbine inlet gas temperature) cannot be measured directly with the present state-of-the-art sensors. Sensing and controlling this parameter is probably the most vital single item necessary to improve reliability and maintainability of modern aircraft. Performance of the engine is basically limited by the need to operate hot metal parts at a temperature that allows long reliable life. Stress creep life is a strong exponential function of temperature. A few minutes of operation at overtemperature conditions can result in dramatic reductions in engine life and potentially catastrophic failure of the turbine. Advanced engines have turbine blades analogous to extremely high response heat exchangers operating with one fluid above the melting temperature of the metal. Turbine blade wall temperatures are a delicate balance between the extremely high heat flux input resulting from the high velocities, pressures and temperature downstream of the nozzle vanes and the cooling airflow within the blades. Only a minimum amount of cooling air is used, since engine performance drops as cooling flow (compressor bleed) is increased. These considerations and experience with present engines strongly indicate that reliability and maintainability factors can be significantly improved by development of a reliable radiation pyrometer system specifically designed to interface with aircraft gas turbine engines.

Measurement of turbine blade temperature not only provides this vital metal temperature but is considered by many engineers to be a more accurate indication of inlet gas temperature than the standard exhaust gas thermocouple harness. Solar

has completed a "Research Analysis of Advanced Sensors for Turbine Inlet Gas Temperature"[1] for the Naval Air Systems Command. Its basic conclusion was that three concepts have the potential to be considered for TIGT (turbine inlet gas temperature) sensors: beta ray probe, ultrasonic air gas and immersed optical target. Formal critiques by turbine engine controls engineers were an integral part of this research analysis of TIGT sensors. (Pratt & Whitney, General Electric, and Allison were among the companies participating.) Of the three systems selected as potential TIGT sensors, none are sufficiently well advanced or miniaturized to be considered as possible sensors for the small low-cost Army aircraft turbines. Analysis of other alternate approaches was made in great detail. All immersion concepts were materials limited above 2000° F. Fluidics, in addition to basic materials problems, had severe contamination sensitivity, since exhaust gas must pass directly through small diameter passages in the oscillators. Accuracy of fluidic elements at high-temperature gas conditions was also found to be greatly dependent upon incorporation of bulky radiation shielding, which was, itself, life-limited above 2000° F. More detail analysis can be obtained on these alternate approaches together with detailed analysis of eight other methods in Reference 1. Throughout the course of this NASC program it became clear that many turbine engineers are convinced that priority should be given to a turbine blade temperature sensor rather than the longer range and much more difficult problem of a TIGT sensor. Additionally, many believe that the first-stage blade temperature is a more accurate parameter from which TIGT can be deduced than the outputs of several thermocouples in the engine exhaust. Justification for this line of reasoning is based upon problems observed with present thermocouple harnesses:

- Even in the exhaust, large point-to-point variations in the gas temperature are observed. Since the thermocouple measures only a point temperature, many probes are necessary to give even reasonably accurate results.

- Thermocouple temperature as a result of drift, radiation losses, recovery factors, and conduction errors is not equal to gas temperature but only proportional.

---

1 Duffy, T. E., et al, "Research Analysis of Advanced Sensors for Turbine Inlet Gas Temperature", conducted by Solar Division of International Harvester Company, San Diego, California, under Naval Air Systems Command Contract N00019-69-C-0574 (June 1969 to July 1970).

- Response of thermocouples is poor, since a type that can have reasonably long life must be relatively massive.

- Turbine performance must be assumed to be constant and known in order to factor exhaust or downstream temperature into the TIGT parameter.

When these shortcomings are considered, the computed TIGT parameter must have an adequate safety margin applied to the answer. Since advanced engine TIGT studies are difficult if not impossible to make, even with laboratory equipment, no firm number can be quoted for the safety margin. Values ranging from 50° to 70° F, however, are estimated. It is reasonable to assume that if the blade temperature is known within ±20° F, TIGT can be estimated with an accuracy much better than ±50° F. This estimate will have a higher degree of reliability and a faster characteristic response than that achieved with an exhaust thermocouple harness.

PERFORMANCE DIAGNOSTIC USES OF TURBINE BLADE TEMPERATURE

Radiant power proportional to the blade temperature is collected from a preselected target area by a sensor head. From the immediate area of the interface of the sensor with the engine, the signal is transmitted by flexible fiber optics to a relatively cool location remote from the turbine case. The radiant power is then converted by a silicon photovoltaic diode to an electrical signal for further processing. It has been determined by system analysis that the three most important temperature intelligence parameters that should be measured are:

1. Average integrated temperature of all blades on a rotor
2. Average of the maximum peak temperatures of all the blades on a rotor
3. Maximum peak temperature of the single hottest blade on a rotor

For flexibility and convenience, these data can be used in three different outputs: a digital display in degrees Fahrenheit; a high response linearized DC output voltage scaled to 1mV = 1° F; or a high response nonlinear signal.

Turbine blade temperature control in engines is one of the most critical factors in the design of an engine. Advanced technology engines operate with turbine inlet gas temperatures well above the safe limits of the metal to achieve low specific fuel consumption and high specific power per unit weight and volume. These engines depend upon diverting compressor discharge air to cool the blades and other hot engine parts. The work added to the compressor air used for blade

cooling is largely lost. Thus, it becomes important to operate the blades as near the maximum temperature allowed by the material life factors. At these high inlet temperatures, 1900° F and above, and with air-cooled blades operating at high-pressure ratios, the temperature response of each blade becomes a critical balance between very high convective heat inputs and internal convective cooling. Under many operating flight conditions the thermal time constant of advanced technology engine blades is less than one second. Thus, conventional methods of preventing overtemperature, previously found to be adequate, are now becoming increasingly less satisfactory. If indirect parameters are used to compute factors to control blade temperatures, a relatively large margin must be provided for hardware safety. Since a few degrees change in gas temperature can significantly affect performance and life, the gains obtained by optimizing the blade temperature control by direct measurement can be potentially decisive for certain aircraft mission requirements. For variable geometry engines, the above factors become less accurate.

From the information contained in the sensor output signal, the basic health of a number of critical engine components or systems can be directly appraised or indirectly deduced. By comparing the average temperature of all the blades on a rotor with controlled condition test stand results, the general condition of a field engine can be established. An envelope of pressure, torque, speed and blade temperature could be established that related limits of performance of an acceptable engine. If blade temperature were used for this criterion, a more accurate general engine status would be possible, since critical blade cooling performance would be directly factored into the engine diagnostic parameters. Cooling system status to the entire rotor or any one blade could be readily diagnosed by means of a blade sensor system. Contamination, fouling, erosion, leakage, blockage, quality control, or other possible cooling system failures would show up differences between average, average peak, and maximum peak blade temperature. For example, if oil or sand and dust were ingested in sufficient quantities into the cooling air system to cause blockage or a general buildup of insulating coatings within the blade passages, the difference between average blade and average peak blade temperature would increase. Differences between these two parameters of as little as 10° F are expected to be readily detectable, and thus slight changes in the cooling air system will be readily detectable. If a single blade were to start to overheat due to cooling blockage or a puncture in a cooling passage (from ingested or upstream objects), the difference between the maximum peak and average peak temperature signals could diagnose these at their earliest stages.

By making a continuous recording of blade temperature data throughout the operating envelope of the engine, an excellent diagnostic analysis of the fuel control

systems' performance could be established. Starts, accelerations, rated power, military power and power level transient operation can be analyzed with respect to the turbine rotor. Comparisons between initial test stand calibrations and field or diagnostic operations will enable end-to-end evaluation of the control system performance.

If a continuous record is maintained by the incorporation of a simple creep life computer, basic life data will be available. A small "black box" that accepts speed and blade temperature inputs can yield data on the creep life remaining on a particular turbine rotor. Thus, effects of surge, hot starts, suspected overtemperature, control system malfunctions, cooling abnormalities, and emergency military power demands can be directly accounted for between major overhauls of the engine. The effects of these overtemperature operating conditions on the creep life and thermal fatigue life can be factored into the maintenance plan before actual failures occur in operation. Continuous monitoring and recording of blade temperatures could thus become a vital part of engine diagnostic and preventive maintenance plans, resulting in greater reliability with greater mean-time-between-overhauls. By incorporation of this relatively inexpensive sensor system, overall maintenance costs would be expected to be significantly improved, at the same time aircraft reliability and availability are increased.

Test cell operation, analysis, control and development can be greatly improved by exact knowledge of the turbine blade temperatures. Effects of changes of any of the engines' operating systems or parameters upon the most critical of all parameters can be immediately and efficiently ascertained. Control system modification or tolerance studies, altitude, inlet distortions, combustor modifications, system damage, salt spray, sand and dust, etc., are just a few test conditions in which blade temperature data would be useful, if not vital. Blade cooling, coating, or other design modifications, of course, require knowledge of the blade temperature. Present blade designs do not lend themselves to installation of thermocouples due to the very thin walls. If thermocouples are installed, they always have an undesirable heat balance effect that modifies the temperature they were intended to measure. Their life is short and installation cost is high. Efficient temperature mapping of air-cooled blades is essentially impossible and significant; compromises are usually made (together with "guesstimates" based upon inadequate data). The development of engine compatible turbine blade pyrometry makes efficient engine analysis possible at relatively low costs. An important side benefit is the ability of a TBTMS system to save engines from destruction if anomalies occur in the control, combustor or cooling system.

CONCLUSIONS

Radiatio· pyrometry has been shown to be an effective turbine engine temperature measuring system capable of accurate, real time applications as part of control systems, diagnostic systems and laboratory development engine instruments.

Potential exists for digital techniques to reduce cost, improve accuracy and increase system flexibility.

Performance limitations of the system derive largely from the amount of signal available from sensors and are largely size related. Limitations of low end temperature measuring range, frequency response and environmental temperature range are inherent with low signal levels. Larger engines, which allow greater probe sizes to be used, would present greater signal levels for processing. Higher level signals reduce error due to amplifier offset and temperature drift. Engines employing air-cooled blades are costly, and installation of radiation pyrometry would represent a highly cost-effective technique for control and protection.

PRINCIPLES OF OPERATION

TURBINE BLADE TEMPERATURE MEASUREMENT SYSTEM

The temperature measurement system views the rotating turbine blades, and by measuring the emitted, electromagnetic radiation, it produces a signal directly proportional to the temperature of the blades. The system is shown schematically in Figure 1. The sensor head containing the optical system is attached to the outer case of the turbine with a clear optical path from the objective aperture to the turbine blades. The area on the blade from which radiation is accepted is called the target area. Energy is radiated from a solid target as a function of its temperature and the emittance of its surface. The sensor head holds the optics in position and provides a stream of purge air to maintain the optical window free from soot, dirt, or other contaminants that would block transmission. The optical system generally consists of a lens or light pipe and aperture to gather the radiation from the blades and define the target area, and a fiber-optic bundle to transmit the radiation to the detector.

Solid-state detectors produce an electrical current proportional to the radiant power incident upon their surface within a spectral band characteristic of the detector. Silicon detectors have been shown to be effective for turbine applications when operated in the photovoltaic mode. Silicon detectors are responsive to radiation between approximately 0.4 and 1.1 microns. The radiation intensity over this spectral band is exponentially proportional to temperature, thus causing the detector to produce a current that changes logarithmically with the target temperature.

The logarithmic current provided to the signal processor varies as a function of time as the blades pass through the optical path of the sensor. The signal processor operates on this signal to extract temperature information of interest, linearizes the signal as a function of temperature and provides linear digital and analog output signals for control, data acquisition, overtemperature protection and direct readout. Information available in the detector output signal includes:

- Average temperature of the blades
- Average leading-edge temperature (assuming the leading edge is the hottest part of each blade)

- Maximum blade temperature (hottest blade)
- Individual blade thermal gradients
- Turbine wheel speed (proportional to blade passing frequency)
- Creep life expended (or remaining), calculated from an integrated temperature-time-stress (speed) equation
- Thermal fatigue from start-up or over-power transients

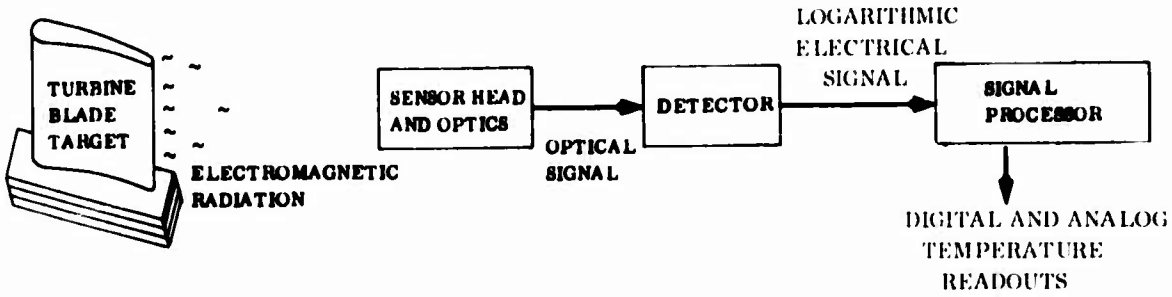

Figure 1. Turbine Blade Temperature Measurement System.

The portion of the available information extracted from the detector signal by the signal processor is dependent on the intended application. Three parameters have been selected as the most meaningful for turbine control:

1. The maximum temperature measured during each revolution (Max. Peak)

2. The average of the maximum individual blade temperatures (Avg. Peak)

3. The average measured temperature (Avg.)

The current design incorporates a digital display of those signals and provides a linear analog signal output.

PHYSICAL LAWS GOVERNING RADIATION PYROMETRY

All matter emits radiant energy to its surroundings as a function of temperature. Solids radiate at all wavelengths; the amount of power radiated at each wavelength is a function of temperature and the surface conditions of the emitting body. A perfect emitter, called a blackbody, absorbs all radiation incident upon its surface. All real surfaces radiate a lesser amount of energy at all wavelengths.

The ratio between blackbody radiation, for which mathematical treatment is available, and the radiation from a real surface is called the emittance.

Radiation from a blackbody, $N_{b\lambda}$, is given by the Planck function.

$$N_{b\lambda} = C_1 \lambda^{-5} \left(\exp (C_2/\lambda T) - 1 \right)^{-1} \quad (1)$$

where $N_{b\lambda}$ = radiance at wavelength λ (watts/cm^2)

T = temperature (°K)

λ = wavelength (cm)

C_1 = constant = 3.7413×10^{-12} (watt cm^2)

C_2 = constant = 1.4388 (cm degree K)

Radiation from a real surface N_λ is found by multiplying $N_{b\lambda}$ by the emissivity, ϵ_λ, which is a function of wavelength and is less than one. A plot of the dependence of radiant power on wavelength for a blackbody ($\epsilon_\lambda = 1$ for all λ) is shown in Figure 2 for several temperatures. The radiant power emitted at all wavelengths increases with increasing temperature. There is a wavelength at which the radiant power is a maximum, and this maximum occurs at shorter wavelengths as the temperature increases, according to Wien's displacement law:

$$\lambda_{max} T = 2897 \text{ micron degrees K} \quad (2)$$

where λ_{max} = Wavelength for maximum radiance (microns)

T = Temperature (°K)

The total amount of energy radiated at all wavelengths increases as the fourth power of temperature according to the Stefan-Bolzmann law:

$$N_{total} = \epsilon_{0-\infty} \sigma T^4 \quad (3)$$

where σ = Stefan-Bolzmann constant = 5.699×10^{-12} watts/cm^2 degree K

$\epsilon_{0-\infty}$ = Total emittance

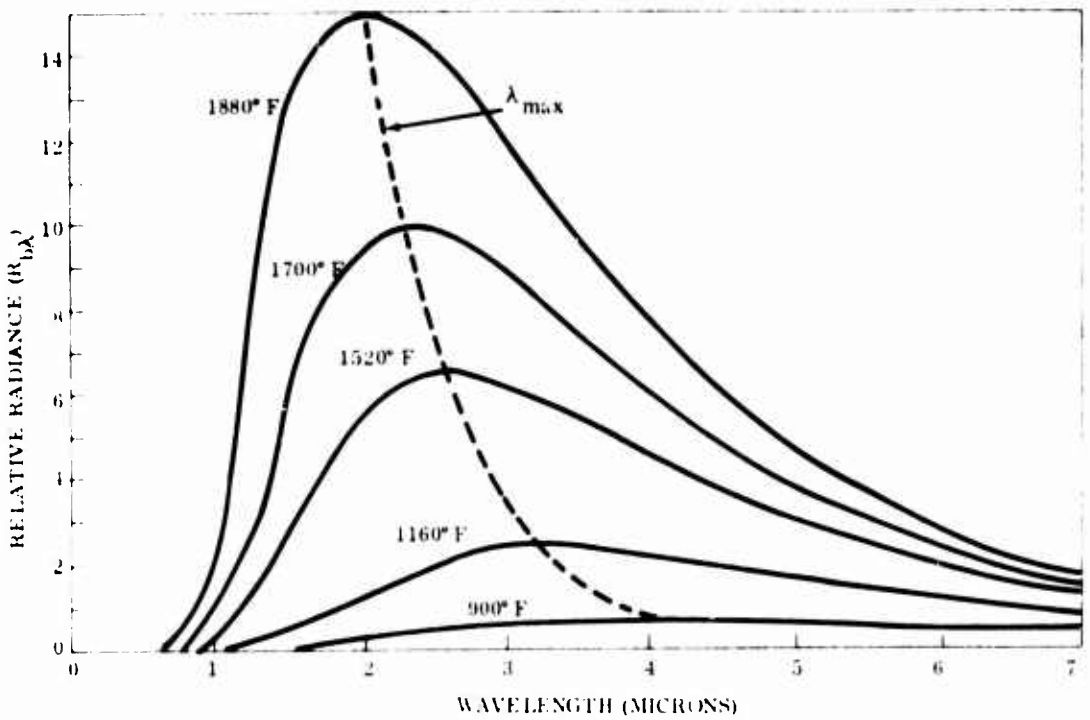

Figure 2. Blackbody Radiance for Several Temperatures.

The radiation emitted by a solid body is approximately given by Wien's equation as a function of wavelength and temperature.

$$N_{b\lambda} = C_1 \lambda^{-5} (\exp - C_2/\lambda T) \tag{4}$$

Wien's equation is within 1 percent of the Planck function for all conditions where

$$\lambda T \leq 3000 \text{ micron degrees Kelvin} \tag{5}$$

thus for wavelengths near 1 micron, Wien's equation holds for temperatures up to 3000° K (2727° C, 4946° F).

The properties of radiation detectors may be more easily analyzed by an exponential equation for the radiance of the type:

$$N_\lambda = \epsilon_\lambda K T^n \tag{6}$$

where K is a constant.

By differentiating and substituting with Wien's equation, the exponent, n, is found to be a function of wavelength and temperature, and is given by:

$$n = C_2/\lambda T \tag{7}$$

Radiation detectors produce a signal, S, proportional to the radiant energy incident upon their surface within their spectral range. The relationship between output signal and target temperature is exhibited by Eq. 6. High sensitivity (large change in signal per unit change in temperature) corresponds to large changes in radiance per unit change in temperature and thus to a high value of n. Equation 7 shows n to be a function of wavelength and temperature. The wavelength used to calculate n is fixed by the spectral range of the detector. A lower wavelength corresponds to a higher value of n and in turn to a signal more responsive to target temperature. The detector output S is given by

$$S = R_\lambda \epsilon_\lambda F N_{b\lambda} \tag{8}$$

where R_λ = Detector responsivity (amps/watt)

F = Optical transfer factor (area^{-1})

Differentiating with respect to temperature derives the following equation for the sensitivity as a fractional change in signal per unit change in temperature:

$$\frac{dS/dT}{S} = nT^{-1}\,\frac{C_2}{\lambda T^2} \tag{9}$$

Sensitivity is directly proportional to the value of n. For detectors that are responsive to a narrow band of wavelengths, an effective wavelength may be calculated to allow the use of the formulas derived for monochromatic radiation.[2] Table I shows the effective wavelength for silicon,[3] the temperature exponent, n, and the calculated sensitivity for silicon detectors.

---

2 Forsyth, W. E., "Optical Pyrometry", Temperature, Its Measurement and Control in Science and Industry, New York: Reinhold Publishing Co., 1941, pp. 1115.

3 Barber, R., and Land, T., "The Place of Photo Voltaic Detectors in Industrial Pyrometry", Temperature, Its Measurement and Control in Science and Industry, Part II, New York: Reinhold Publishing Co., 1962, pp. 391.

TABLE I. DATA FOR SILICON DETECTORS				
Temperature		Effective Wavelength	Temperature Exponent	Sensitivity
(°F)	(°C)	(μ)	(n)	(%/° F)
932	500	0.98	19.0	2.5
1832	1000	0.91	12.4	1.0
2732	1500	0.86	9.6	0.5

Detectors with high values of n are also insensitive to changes or uncertainties in target emittance or optical transfer factor, F. The optical transfer factor is a proportionality constant relating the radiance (watts per unit area) leaving the target to the power (watts) arriving at the detector. The transfer factor takes in account target areas, lens areas, loss in the optical system and view distance. A pyrometer is calibrated at known conditions of emittance (ϵ_c) and transfer factor (F_c). If in use, the emittance (ϵ) or the transfer factor (F) is not equal to the values at calibration, an error in indicated temperature (T_i) will result. The magnitude of the error is shown by differentiating Eq. 8 with respect to ϵ and F. The fractional error between indicated and true temperature is given by:

$$\frac{T - T_i}{T_i} = \left(\frac{\epsilon_c}{\epsilon}\right)^{1/n} \left(\frac{F_c}{F_t}\right)^{1/n} - 1$$

If $\epsilon = \epsilon_c$ and $F_t = F_c$, $T_i = T$ and there is no error. The higher the value of n, the lower the resulting error from a given change in emittance or optical conditions. Table II shows the temperature error for three values of n. For a total radiation pyrometer n is equal to 4. Values of n from 10 to 20 are typical of silicon detectors. A 10-percent error in emittance ($\epsilon_c/\epsilon = 0.9$) produces only a 0.6 to 1.1 percent error in indicated temperature.

TABLE II. ERROR DUE TO INCORRECT EMITTANCE				
ϵ_c/ϵ	Temperature Error (%)			Remarks
	n = 4	n = 10	n = 20	
2.0	18	7	3.5	$T > T_i$
1.0	0	0	0	$T = T_i$
0.5	16	7	3.5	$T < T_i$

Another possible source of error is interaction of the radiated signal with the hot turbine gas flowing between the turbine blade and the optical system. Especially critical are the absorption and emission bands characteristic of the constituent species in the turbine gas. Principal components are H_2O, CO, CO_2, and unburned fuel. Figure 3 shows the radiance from an 1852° F blackbody target, the emitted radiation from the gas, and the spectral range of silicon detectors as a function of wavelength. Silicon has a peak responsivity at approximately 0.85 micron, and significant acceptance of radiation from approximately 0.4 to 1.1 microns. This spectral region avoids all of the absorption and emission from the turbine gases.

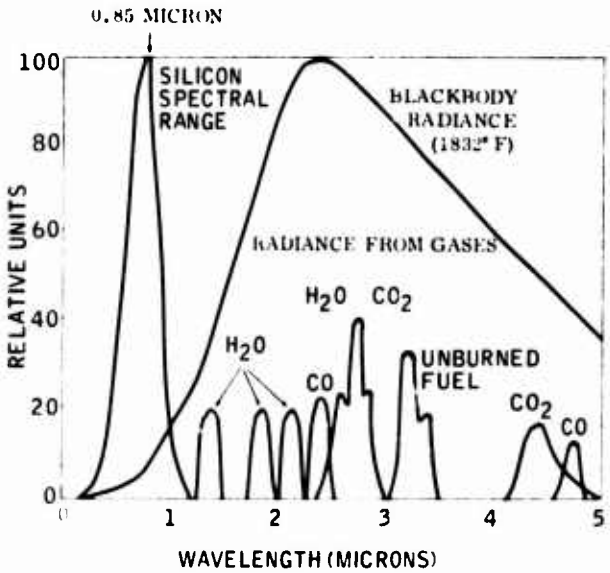

Figure 3. Spectral Response of Silicon and Radiance From Blackbody and Turbine Gases.

RADIATION DETECTOR

The key component in a radiation pyrometer is the detector that transduces optical radiation into an electrical signal. The parameters, properties and characteristics of the detector define, to a large extent, the performance of the entire temperature measurement system. A brightness pyrometer measures the intensity of the radiation incident on the detector. Each type of detector is sensitive to radiation in a different range of wavelengths. Several phenomenological parameters are in general use to describe the performance of radiation detectors.[4]

4 Jones, R. Clark, "Phenomenological Description of the Response and Detecting Ability of Radiation Detectors", Proceedings of the IRE, Sept. 1959, pp. 1495-1502.

Most detectors are used in a range where output is proportional to input. The ratio of output-to-input is called the responsivity, R_λ. The units of responsivity are volts per watt. In the case of photovoltaic sensors operated in the short-circuited mode, responsivity given in amps per watt is more useful. The term sensitivity is also often used in place of responsivity, but its general use for a number of related concepts makes it somewhat ambiguous. The responsivity of a detector relates output to input but does not give any information as to how small a signal can be measured.

The minimum measurable signal is controlled by the level of the electrical noise in the output signal. If the rms voltage of the noise is divided by the responsivity (in volts per watt), the noise equivalent power (NEP) of the detector results. The noise equivalent power is numerically equal to the radiant input power needed to produce a greater output signal from a given radiant input than a less responsive detector. A detector with a smaller noise equivalent power will have a greater detecting ability. The reciprocal of the noise equivalent power, called the detectivity, is thus a direct measure of the detecting ability of the detector. Noise equivalent power and detectivity are complex and ill-defined functions of a number of variables such as detector area, frequency, temperature, gain and power level. Each parameter must be specified in a standard condition to allow comparison of one detector with another. Detectivity is usually specified "in the reference condition E" and is written as D*. Detectivity (D*) is shown in Figure 4 as a function of wavelength, λ, for several detectors. The spectral response characteristics of each type detector are readily apparent. Silicon is seen to have a very high detectivity and a narrow spectral bandwidth.

Silicon radiation detectors have been used almost exclusively during the development of the TBTMS. Silicon detectors from several manufacturers have been tested and evaluated. No one detector manufacturer has proven to have an optimum detector for this application. Detectors must be rugged and small, and have low capacitance for the highest frequency response. Also, the detectors must display a reasonably linear change in output as a function of temperature. This is discussed in more detail in the section titled "Signal Processor".

Among silicon detectors there are three main types: surface barriers, diffused junction and lithium drifted. The active junction is usually formed by depositing a thin film of gold on the surface of n silicon for surface barrier type detectors. A diffused diode is produced by diffusion of an impurity into n or p type silicon to produce an n-p junction. The active area of the third type is an intrinsic region of silicon produced by the diffusion of lithium in n type silicon. The three types of detectors have different responsivity to radiation over the wavelength of interest. Thus, one type must be chosen and used consistently once a calibration curve has

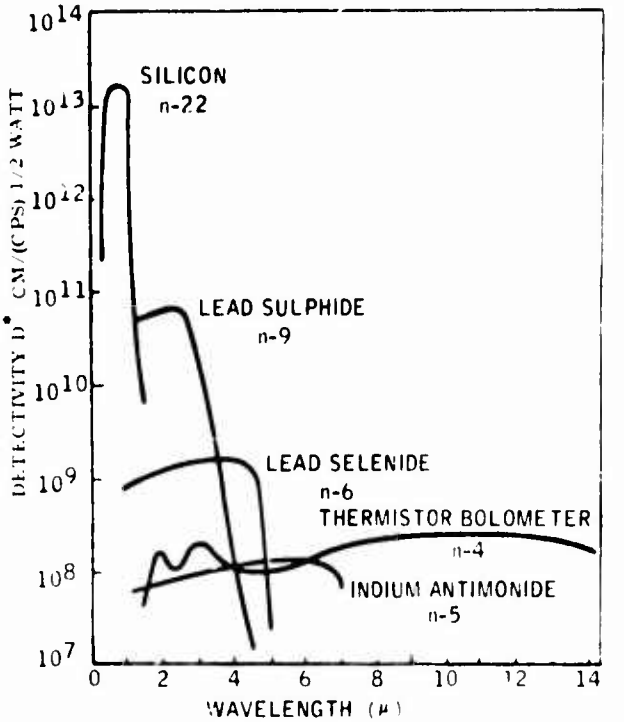

Figure 4. Detectivity (D*) for Several Detectors (Ref. 4).

been developed and incorporated into the electronic signal processor. Because of a stronger "blue" response and a tendency toward instabilities, the surface barrier type detectors have not been used. Lithium drifted detectors must be cooled at all times to avoid further drifting. A practical TBTMS cannot use such a detector. The diffused junction detectors have proved to be dependable and reliable in this application. Among the diffused junction detectors tested, the calibration curve (output current versus turbine blade temperature) remains within a few percent. Figure 5 shows a typical calibration curve.

The calibration is accomplished with a heated strip target, a sensor head, filter optic cable, a detector and an amplifier. The thermal radiation is transmitted from the temperature controlled target to the detector via the sensor head and converted to a current at the detector. The electrical current is run into an operational amplifier which produces a voltage output. Normal detector current levels range from 10^{-8} to 10^{-5} amperes. To eliminate losing the small signal in detector dark current, the detector is operated unbiased (photovoltaically). The operational amplifier configuration simulates a short circuit configuration for the detector which has been shown to result in the greatest signal stability over the operating temperature.

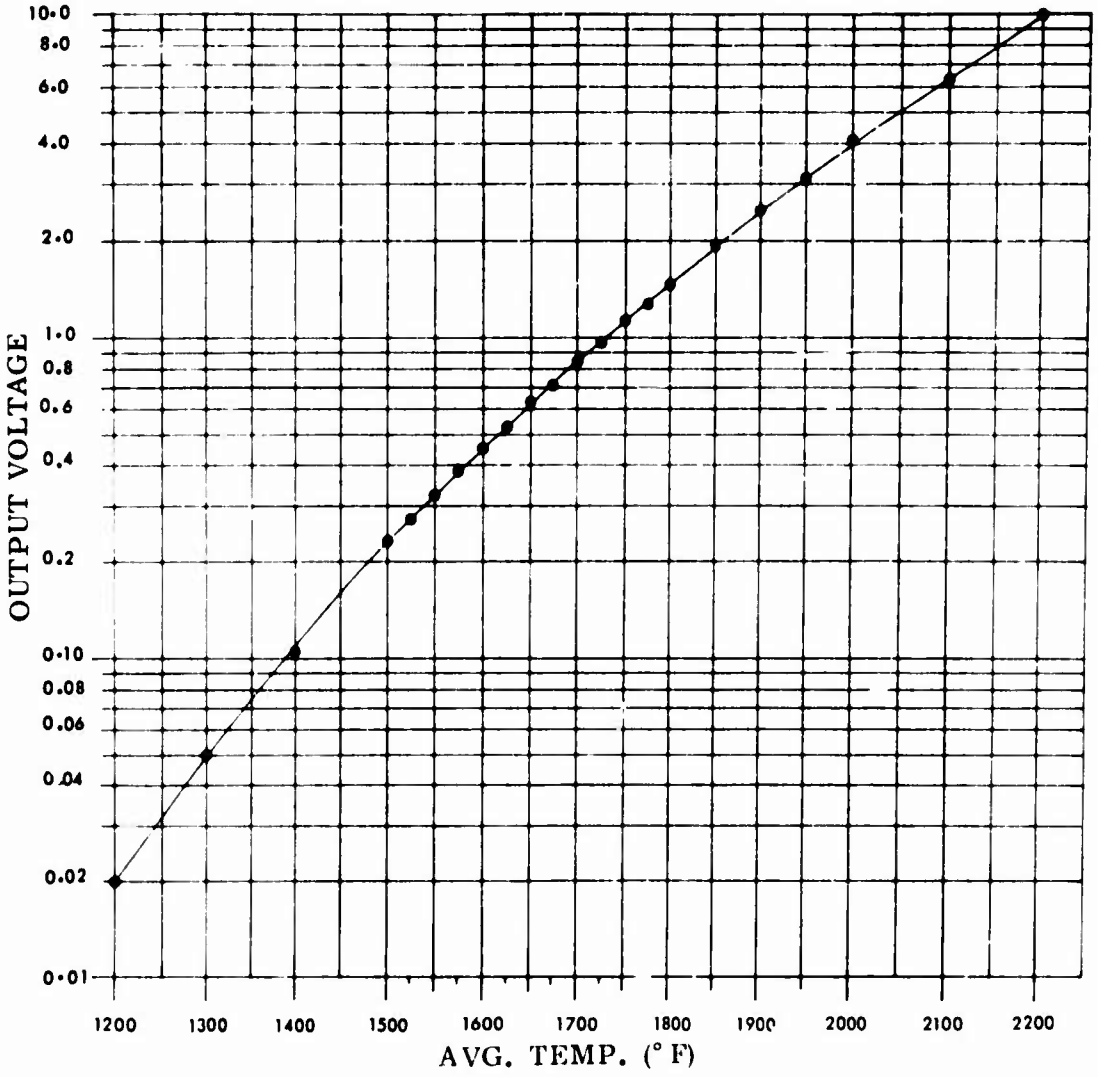

Figure 5. Detector Output Voltage Curve on Semi-Log Scale.

The main problem associated with the use of silicon detectors is drift in the output signal due to changing environmental temperatures. As the environmental temperature of the silicon detector is increased, its generated output current will rise independent of radiant power input. Most of the increase in current output results from a decrease in photon energy needed to break the valence bond within the junction. Thus, the spectral response is enhanced at long wavelengths when the detector is warm. The current generated increases approximately linearly at a rate of 0.25 percent per degree Fahrenheit in the range from -50° to 125° C. Solutions to this problem are discussed in the section titled "Signal Processor".

In general, the silicon detectors are small, rugged, require no external power supplies, and are sensitive to radiation in a narrow spectral region that is devoid

of gas absorption or emission peaks. Operation to 250° F is practical, and over-temperature of 300° F has been experienced with no appreciable degradation. Because of severe signal compensation problems, operation at temperatures over 220°F is not recommended.

OPTICAL SYSTEM

The purpose of the optical system is to define the target area on the surface of the blades and to direct the radiant energy onto the detector. Remote placement of the detector due to its limited temperature capabilities makes the use of a light pipe or fiber-optic bundle necessary. The sensor head holds the objective end of the optical system in the proper geometric relationship to the target and provides an interface between the optic and the engine. Purge air flowing through the sensor head maintains the cleanliness of the objective window.

There are two basic types of optical systems applicable to turbine blade temperature measurement systems. Figure 6 shows a schematic diagram of lens and light pipe optical systems with the principal environmental temperature zones imposed by the engine. A lens system, Figure 6(A), uses an objective lens to focus the radiation onto a field aperture which defines the target size and shape. The radiation is then transmitted to the cooled detector by a solid light pipe, a flexible fiber-optic bundle, or a combination of the two. Typical objective aperture diameter is 0.4 inch with 0.1–0.25-inch target diameters. Figure 6(B) shows a light pipe system where the radiation is accepted by the light pipe within a cone of half angle usually equal to 15-30 degrees, thus defining a target area on the blade surface. In comparison with the lens system, the objective aperture of a light pipe system is small, typically 0.060-inch diameter; and the target area is large, 0.3-0.5 inch. The temperature imposed on each section of the optics is shown in Figure 6.

LENS SENSOR

The objective lens focuses radiation from the target onto the fiber-optic bundle. Focal length, geometry, and the size of the field aperture opening define the target size. The radiant power incident on a detector through such a sensor head upon the silicon detector is

$$\phi = F\epsilon N_{b\lambda}(T) \tag{10}$$

where F is an optical transfer function for both the lens, and fiber optics, ϵ, is the emissivity of the turbine blade, and $N_{b\lambda}(T)$ is the power radiated from a blackbody at temperature, T.

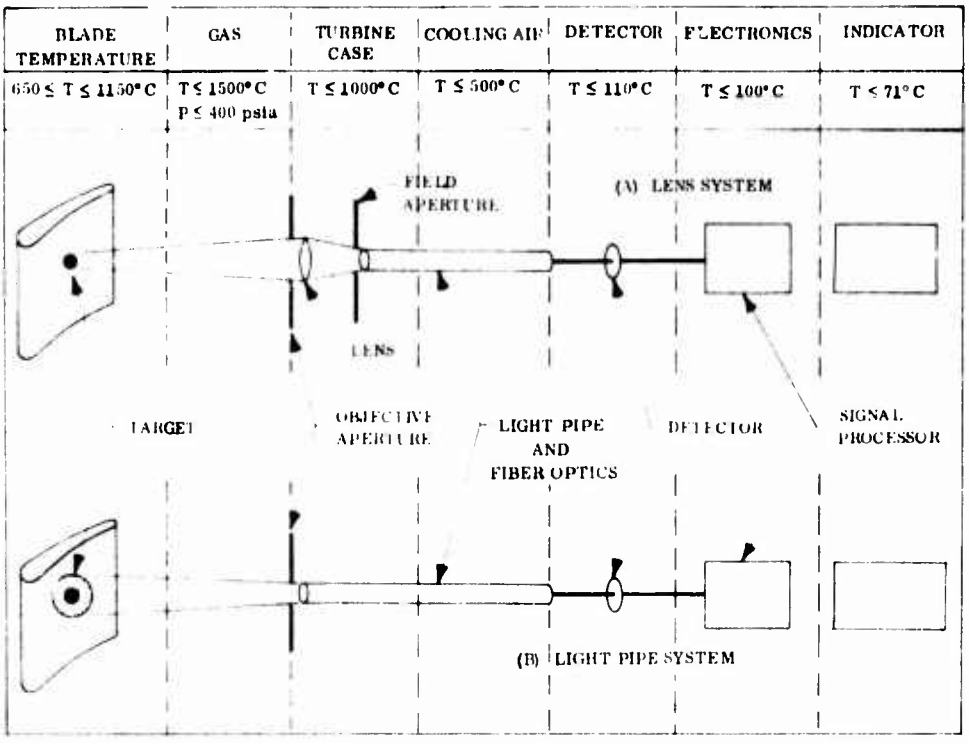

Figure 6. Environmental Zones Imposed by the Turbine Engine on the Lens and Light Pipe Optical Systems.

A high value for the transfer factor signifies a higher signal and thus a lower minimum temperature capability for the system. From an operational standpoint, however, small objective lens and target areas, as well as long target-to-lens distances, are preferred. The conflicting criteria must be compromised for each type of engine and application.

The objective lens may be made from fused quartz or sapphire. These materials combine the necessary high-temperature capabilities with high transmission in the near infrared. The lens diameter and focal length are, in general, made as small as possible. Diameters of 1/2 inch are typical.

APERTURE SENSOR

The aperture sensor accepts thermal radiation from a relatively large area of the turbine blade. The radiation energy passes through the aperture and is incident on a fiber-optic cable. A silicon detector is placed at the end of the fiber optics. The target area is defined by the distance from the target to the aperture, the aperture size, and the distance from the aperture to the light pipe.

In some cases the acceptance angle of the fiber-optic light pipe affects the area of the target that is monitored. In a typical installation, the aperture is 0.040 inch in diameter, between 1 and 2 inches from the target and 0.3 inch from the light pipe. Purge air bleed through this sensor prevents the buildup of soot on the optical components and cools the aperture to prevent it from radiating and thus influencing the signal.

Although the aperture sensor receives radiation from a large target area, it is preferred in many engine applications over the lens sensor, which can accurately measure the temperature of a small spot (typically 0.150 inch in diameter).

STATOR SENSOR

A stator sensor has been developed which is based on the same physical laws as the other sensor types and uses the same signal conditioning to produce an electrical signal output. This sensor is designed for measuring the temperature of stators or other engine hardware at two positions simultaneously. The radiant energy is transported via fiber-optic rods to two silicon detectors mounted in the upper bell-shaped portion of the sensor assembly.

SIGNAL PROCESSOR

GENERAL DESCRIPTION

The signal processor accepts the signal from the silicon radiation detector and converts it into useful engineering data with a readout in millivolts directly proportional to temperature in degrees Fahrenheit (1mV = 1° F).

The functions of the signal processor include:

- Converting the detector current signal into a voltage
- Amplifying the signal
- Compensating for thermal shift in detector output
- Filtering noise from the signal
- Detecting peak voltage
- Linearizing silicon detector output
- Displaying and producing output in degrees Fahrenheit

These functions are performed with the electronic hardware built into the signal processor (Solar P/N 106988). The signal processor and its front panel design are shown in Figure 7. The principles of the operation are described below.

System Design

The functional components of the signal processor and their arrangement are shown in Figure 8. An N on P silicon photovoltaic detector is the first element in this system. Photons are transduced to a microampere signal by the solid state energy converter.

The current output from the detector is converted by a preamplifier to a voltage. The preamplifier, located next to the detector, has a frequency response of 50 kHz to prevent signal attenuation at the high input frequencies resulting from blade passing rates of up to 20,000 blades per second. Normally, each type of sensor head produces a different output current at a given target temperature. Thus, a gain adjustment is provided on the main amplifier that allows each sensor head to be calibrated directly in degrees Fahrenheit.

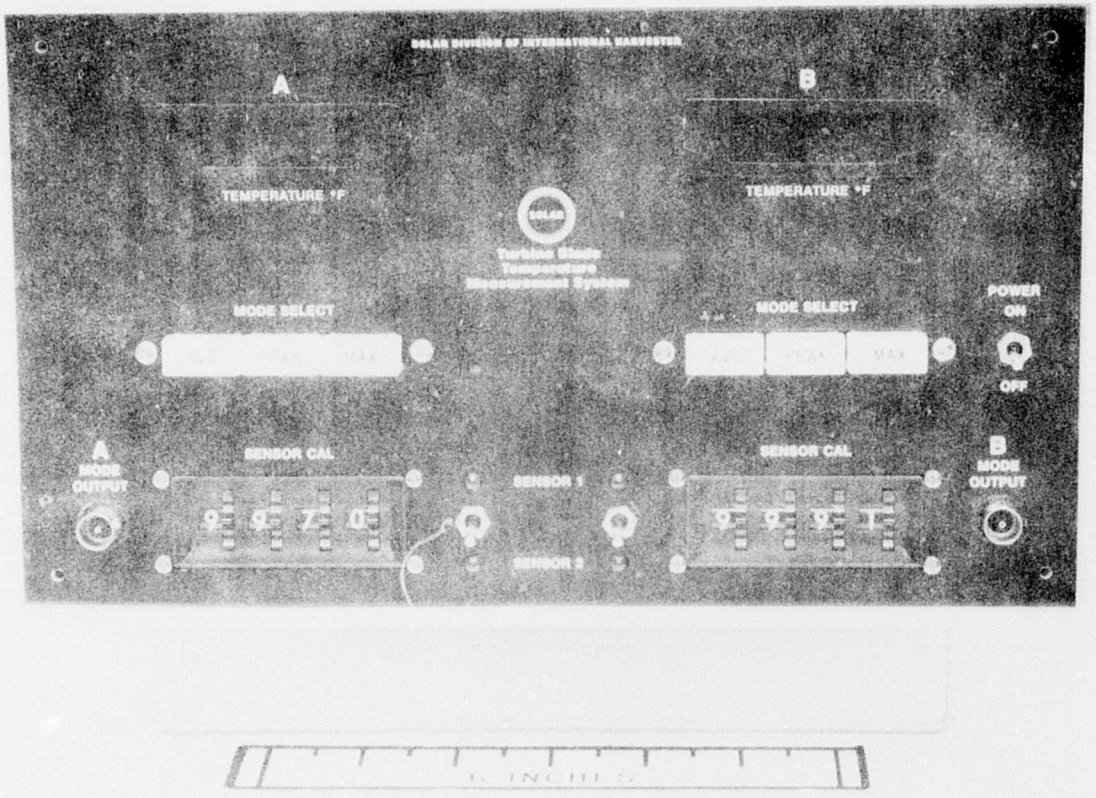

Figure 7. Signal Processor Front Panel.

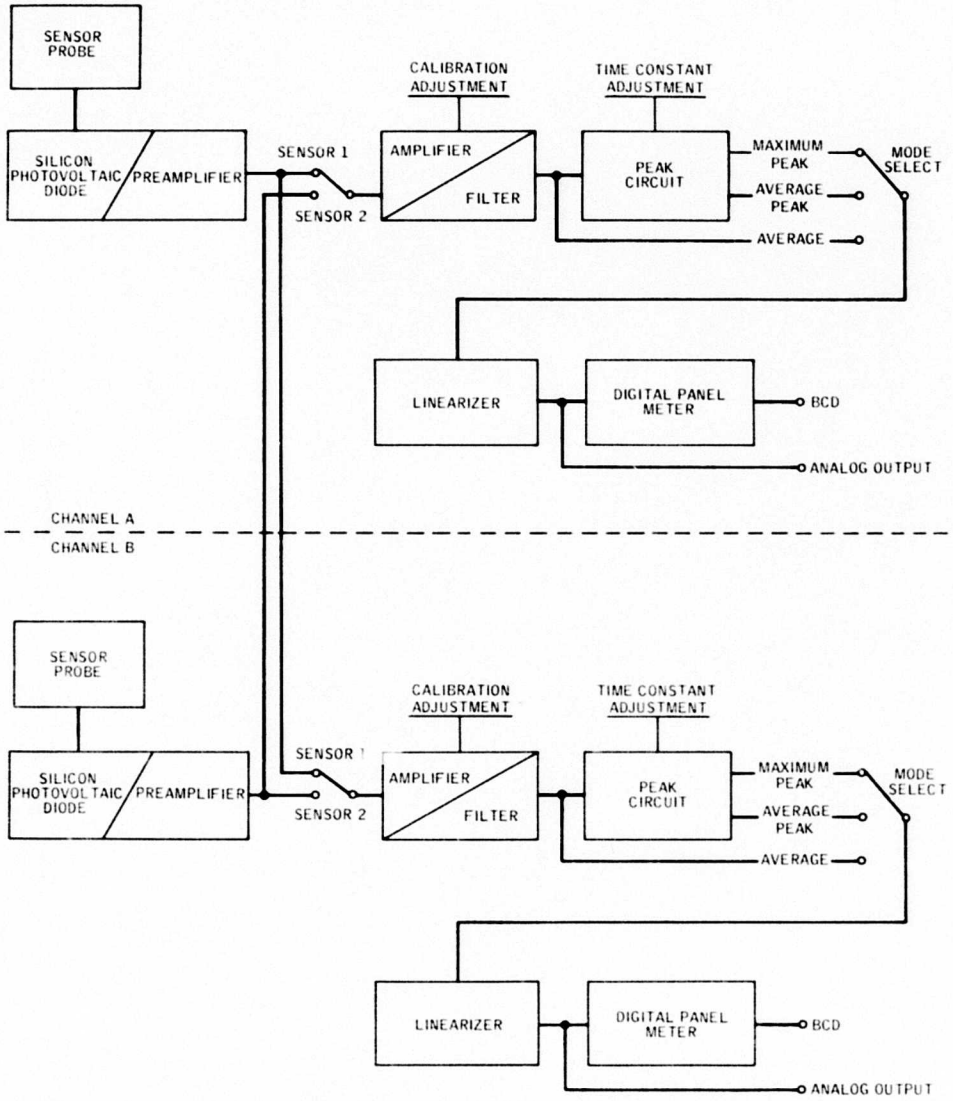

Figure 8. TBTMS Readout and Control Functional Block Diagram.

From the main amplifier the signal goes to the temperature mode selector switch. By positioning the switch, an average, an average peak, or a maximum peak voltage circuit is placed in series with the rest of the system. In the average circuit the signal is transmitted directly to the output amplifier without further operations performed on its wave form. In the average voltage mode the peaks of the voltage wave train are held with a peak voltage hold circuit designed to maintain the voltage between each peak at approximately the average level. On Figure 9, this voltage

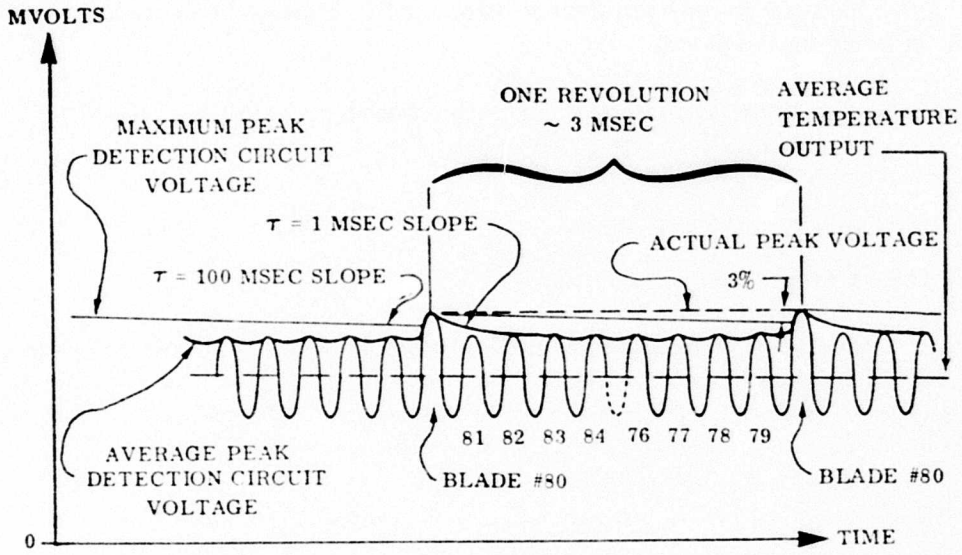

Figure 9. Voltage Detection and Analysis Circuit Outputs.

level is shown by the interconnecting lines between each of the wave peaks representing the blade-to-blade output voltage. In the maximum peak temperature mode the electronic circuit switched into the system will maintain the maximum peak voltage of the hottest blade in the pulse train. The top voltage trace in Figure 9 depicts the maximum voltage level which is proportional to the blade on a wheel with the highest temperature. Each of the peak detection circuits has an adjustable hold time.

Typical turbine blade passing frequencies are as high as 20,000 blades per second, or as low as 5,000 blades per second. The basic method used to hold the voltage is to charge a capacitor through a diode and hold this voltage for a predetermined time by closed-loop operational amplifier circuits. If the voltage is held for 1 or 2 milliseconds, an average peak voltage is obtained. By holding for 100 milliseconds, the maximum peak voltage will be held. Figure 9 illustrates the output of the peak hold circuits with a 3-percent drop.

The rise time of the peak circuit is about 1 microsecond. Thus, the current will charge to the maximum of each blade voltage pulse. As the voltage drops after reaching the peak (the blade passes out of the optical axis), the voltage is prevented from dropping by the blocking diode. A controlled discharge rate is obtained by shunting the capacitor with a high resistance. By fixing the circuit time constant to match either turbine blade frequency passage or rotor rpm, the

circuits can be made to hold a voltage proportional to average blade temperature or hottest blade temperature.

Typical response of the signal output for each mode is as follows:

AVG, τ $<10\mu$sec

AVG PEAK, τ $\cong$1 to 3 msec

MAX PEAK, τ $\cong$50 to 200 msec

The signal output of the amplifier and mode control is highly nonlinear with temperature. A "high response" output at this point allows the operator to view the actual wave form which is similar to that in Figure 9. Intelligent interpretation of this display can help in diagnosis or development work on gas turbine engines. For control and visual interpretation it is useful to have a linear output directly proportional to turbine blade temperature. The components following the amplifier perform these functions. The linearizer produces a signal proportional to temperature (1mV = 1° F) in the range of 1200° F to 2200° F. Linearizer response time is less than 5 msec. At this stage the signal can be diverted to either display units, feed an engine control scheme or both.

DETECTORS

The silicon detectors used in the TBTMS must be rugged and small and have high frequency response and linear thermal drift characteristics. No one detector brand has all of the desired features. The two most important tests, temperature drift and frequency response, have been performed on detectors from four or more manufacturers. These detectors all had the same spectral response but varied in construction from unmounted to completely encased. They were tested for frequency response and thermal drift. It has been found through experience that the unmounted detectors are the smallest and most rugged, especially when custom mounted into the preamplifier assembly. Factory mounted detectors are not assembled for use over a wide temperature range. Most of these detectors fail at extreme temperatures due to bonding, wiring and mounting problems.

PREAMPLIFIERS

The concept of building a preamplifer into the detector housing to increase the line driving power and noise suppression has been employed. Each sensor head has a built-in detector-preamplifier that is individually temperature compensated up to 220° F. No further adjustments can be made.

System Design

The complete dual channel TBTMS signal processor has been built using the components described above. The preamplifiers are used as individual components, and the circuits have been incorporated into a four-board TBTMS. Two boards forming one channel are shown in Figure 10.

System Performance

Fundamental performance goals were as follows:

- Range and Accuracy: ±10° F (±5° C) from 1400° to 2100° F (760° C to 1150° C) when calibrated with an electrically heated flat metal strip target made of oxidized Hastelloy X foil. Expected installed accuracy ±2 percent of full scale.

- Frequency Response: DC to 50 kHz (-3 dB) for composite signal 90 percent DC, 10 percent AC pk-pk.

- Environmental temperature range (preamps) -40° F to 230° F (-40° C to +110° C).

In order to meet or come as close to the design goals as possible, a number of compromises had to be made. It is the nature of smaller turbine engines that necessitates the use of smaller probes. The probes designed for the Titan T62T-32 when connected to the signal processor for the first time clearly showed that large gain increases were required for the aperture and stator sensors to properly process the signals. A number of high gain, wide band operational amplifiers which had recently come on the market were purchased and examined for the application. Among these, one exhibited excellent gain and frequency response; however, noise levels in the current-to-voltage mode were excessive. The noise in the average mode is not troublesome; however in average peak and maximum peak modes, this noise is captured. As a result, the individual blade signal information is obscured. A second device likewise reacted unfavorably in the current-to-voltage mode. There was a tendency to oscillate, and it had a large offset voltage which interfered with basic accuracy.

The stability, low noise, gain and frequency response of a third amplifier in the current-to-voltage mode was found to be acceptable for the system.

It is important to realize that the basic characteristics of the measuring system are fixed by the preamplifier stage.

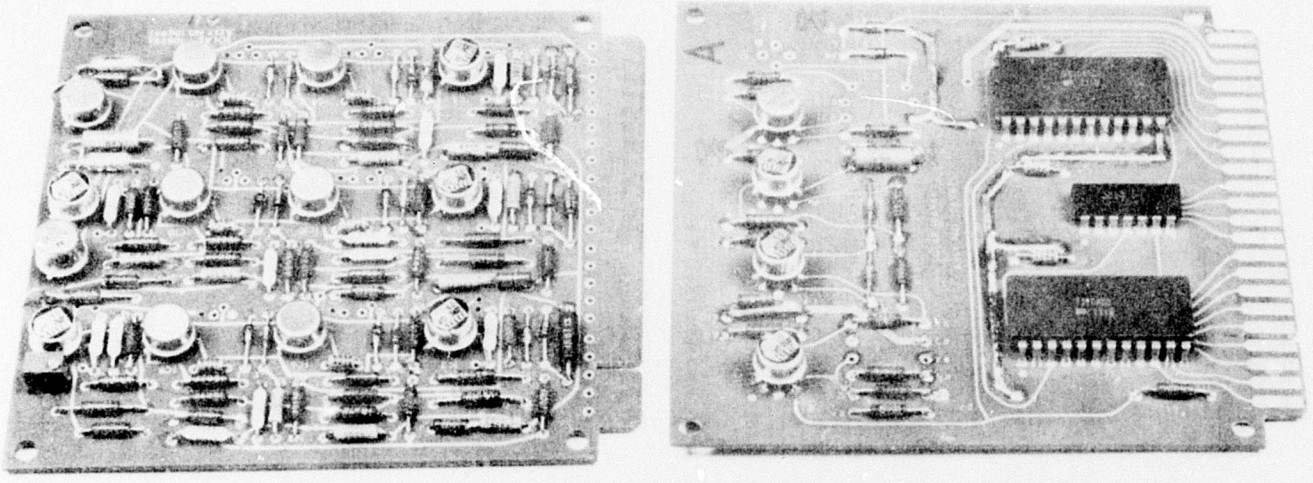

Figure 10. Printed Circuit Boards of Channel A.

After bench and engine tests and after an examination of those devices which appeared from specifications to offer superior performance, the following performance was achieved:

- Range and Accuracy: ±10° F (±5° C) from 1400° F to 2100° F (760° C to 1150° C)
- Frequency Response: DC to 54 kHz (-3 dB)
- Environmental temperature range (preamps) -40° F to 230° F (-40° C to +110° C)

The data in Table III are representative of bench test data for the optical pyrometer system.

TABLE III

BENCH TEST DATA

Accuracy - Strip Target Calibration

Strip Target (° F)	Channel A Readout (° F)
2100	2108
2050	2048
2000	1996
1950	1948
1900	1894
1850	1849
1800	1794
1750	1745
1700	1698
1650	1649
1600	1600
1550	1548
1500	1505
1450	1448
1400	1395
1350	1344
1300	1294
1250	1230
1200	1174

Frequency Response - Electronic Simulator

Input (kHz)	Channel A Output (dB)
10	0
15	+0.3
20	+0.65
25	+0.8
30	+0.9
35	+0.75
40	+0.15
41	0
42	-0.2
43	-0.35
44	-0.60
45	-0.80
46	-1.0
47	-1.3
48	-1.5
49	-1.8
50	-1.95
51	-2.0
52	-2.5
53	-2.7
54	-3.0
55	-3.3

System Operation

The front panel of the turbine blade temperature measuring system is shown in Figure 7. Reference to this figure will aid in the explanation of the front panel control switches and readouts.

The signal processor front panel is divided into two channels, Channel A and B. The two channels are capable of independent signal processing of two sensor heads or simultaneous signal processing of one sensor head. Independent signal processing is most likely to be used when the application involves two distinct sensors targeted on separate areas in the power turbine section of an engine. Channel B has a higher amplification than Channel A. The lens sensor is used on Channel A, the aperture on Channel B, and the two outputs of the stator sensor are routed to both channels. The stator sensor of this program targets on the leading edge and trailing edge of two separate guide vanes in the engine nozzle.

To operate Channel A, connect preamplifier output cable to sensor 1 or sensor 2 input connector on rear of instrument. Move power switch, located at right-hand side of panel, to On. Move Channel A sensor switch to center position. Verify that digital panel meter reads 1020° ±7° F. Move sensor switch to sensor 1 or sensor 2 position to match preamplifier connection. Set thumbwheel selector switch to number marked on side of preamplifier in order to calibrate system. Depress the mode select switch desired to examine turbine blade characteristics. Mode select switches are lockout type, which negates chances of depressing two switches simultaneously. With the engine operating and the turbine blade temperature within instrument range, the digital panel meter will display a four-digit temperature value in degrees Fahrenheit.

Operation of Channel B is similar to that of Channel A. With the increased gain of Channel B, approximately ten times that of Channel A, there is increased susceptibility to preamplifier offsets and drifts. For this reason, Channel B should be used for low output sensors that require high gain, such as the aperture sensor, the difficulty being one of achieving high gain, wide frequency response, low noise, low offset voltage and low voltage drift. To date, an amplifier has not been found which meets all of these characteristics to the necessary degree.

Located in the lower left- and right-hand corners of the front panel are BNC mode output jacks. By connecting an oscilloscope, an examination of the output wave form may be made and photographs taken.

Located on the rear panel are the linear output jacks, BCD connectors, preamplifier input connectors and power receptacle with fuse holder.

Calibration

Calibration is best achieved with an electrically heated flat metal strip target made of oxidized Hastelloy X foil. A reasonably thick strip on the order of 0.030 inch is less susceptible to air currents. A type S thermocouple is imbedded just below the surface from the backside and connected to a thermocouple digital readout with four-digit resolution. A comparison between the thermocouple readout and the pyrometer signal processor is initially done at 1600° F. The thumbwheel switch is adjusted up or down in order that the readings match. The four-digit number should match the preamplifier housing calibration number. Figure 11 is a diagram of end-to-end calibration test.

Alternatively, calibration can be achieved using a blackbody radiation source.

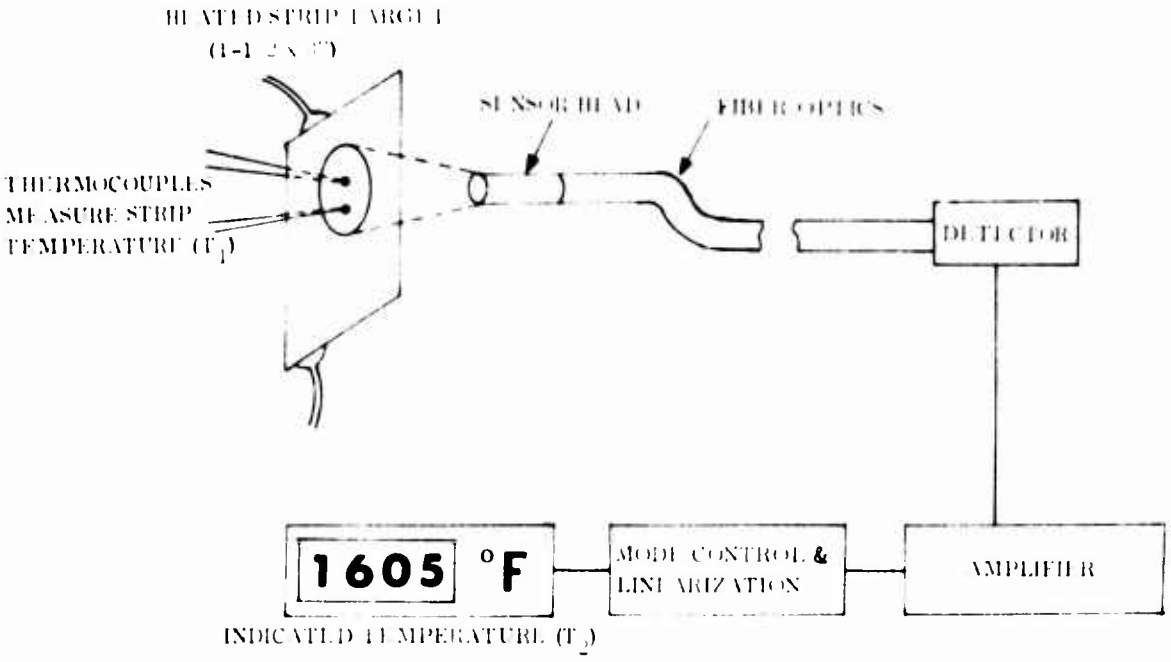

Figure 11. Diagram of End-to-End Calibration Test.

SENSOR HEAD AND OPTICS

GENERAL DESCRIPTION

Three sensor designs were developed under this program to examine the power turbine radiation characteristics of a Titan T62T-32. The sensors developed consist of lens, aperture, and stator adapters which, combined with the probe, view the turbine wheel and selected parts of the nozzle vanes. Figure 12 shows the probe used to gain optical access to the nozzle and turbine wheel through the air inlet housing. Figure 13 shows the probe installed with the combustor removed.

Figure 14 shows the lens and aperture adapters. Figure 15 shows a view of the stator sensor. A unique feature of the stator sensor is the optical path which has been shortened through the use of glass rods and placement of the electronics in proximity to the target. This necessitates cooling of the electronic area with shop air.

FIBER-OPTIC CABLE

The fiber-optic cables used are 3/16 inch corner to corner, coherent, bundled glass rods, 3 feet long. Solar-designed end fittings are used to connect the preamplifier housing to the fiber-optic cable and to the sensor probe. The cables are armored with a flexible spiral wrap formed from stainless steel. A small "O" ring is used to seal between the preamplifier housing and the cable fitting. Provision has been made also for lockwiring the cable connection points.

SENSOR DESIGN

The lens sensor characteristically examines a small spot (0.2 inch) on the turbine wheel. For ease of design, a lens of 5 mm diameter and focal length of 317 mm (1.25 inch) has been used on many programs. The lens' characteristics therefore are a starting point. Knowing the focal length, we calculate the lens position as follows:

$$1.25 = \frac{(x_1)\ (x_2)}{x_1 + x_2}$$

$$1.25 = \frac{(x_1)\ (6.60 - x)}{6.60}$$

6.6 inches = total distance

x_1 = front of lens to target

x_2 = front of lens to aperture

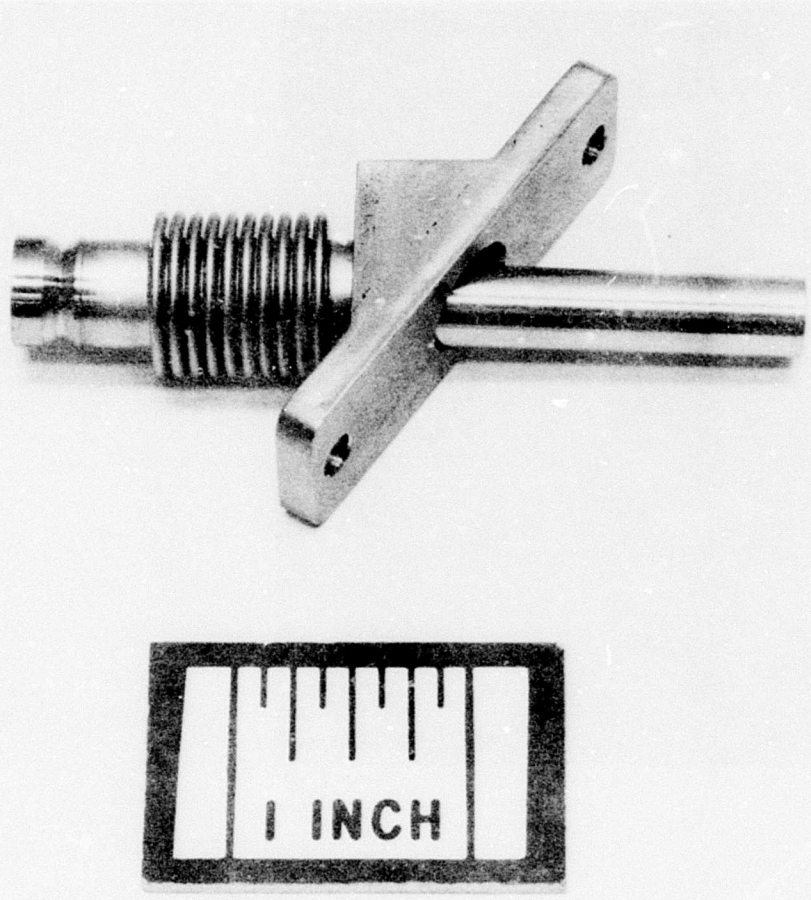

Figure 12. T32 Probe.

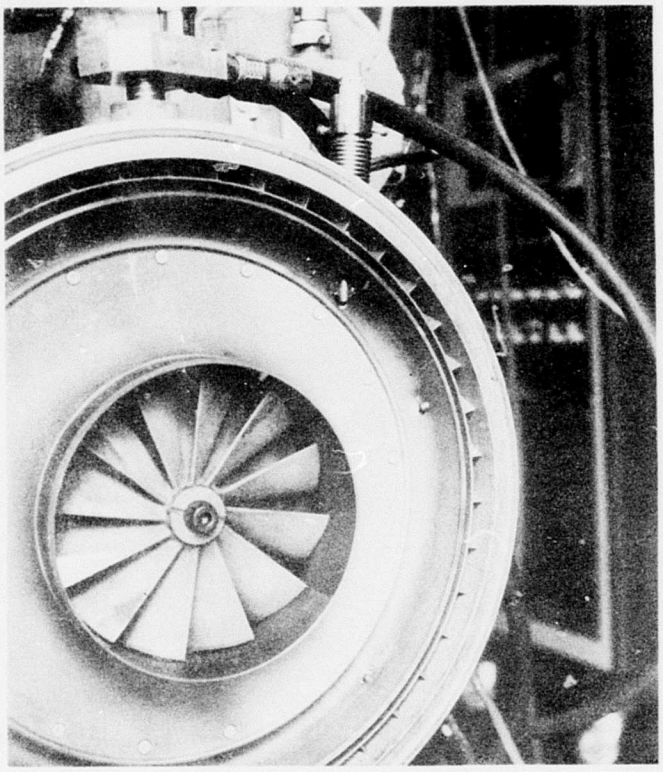

Figure 13. Installed Probe in T62T-32 With Combustor Removed.

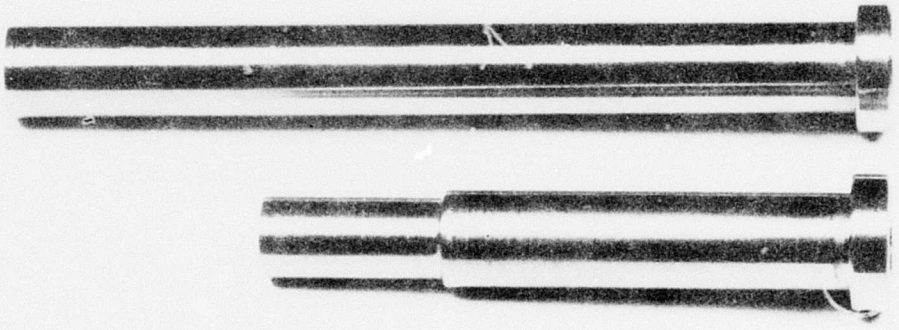

Figure 14. Lens and Aperture Sensor Adapters.

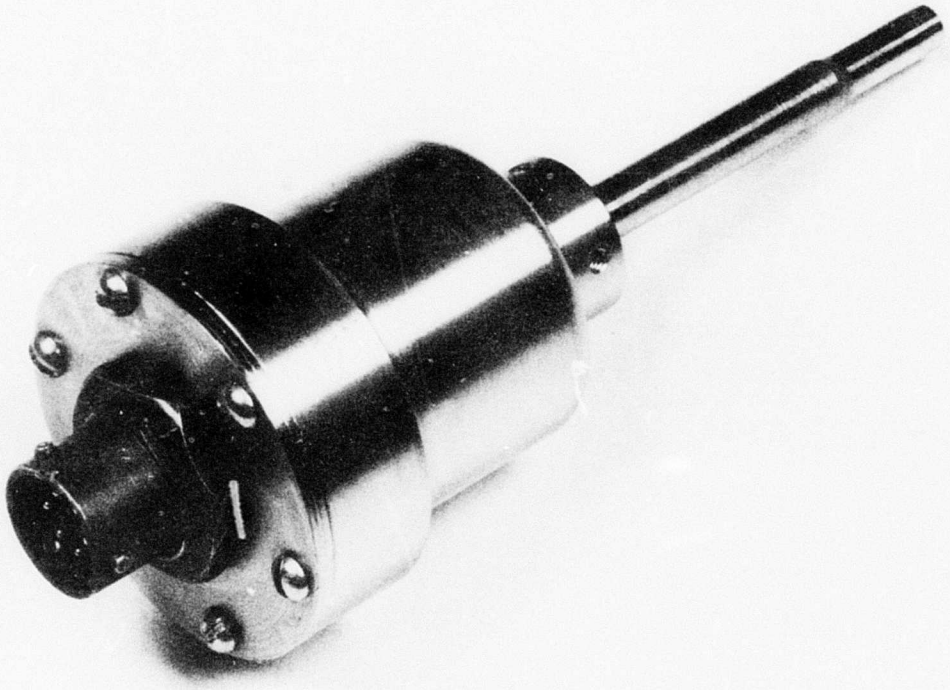

Figure 15. Stator Sensor Adapter.

$$x^2 - 6.60x + 8.25 = 0$$

using quadratic equation:

$$x = \frac{b \pm \sqrt{b^2 - 4ac}}{2a}$$

$$= \frac{6.6 \pm \sqrt{(6.6)^2 - 4(8.25)}}{2}$$

$$= \frac{6.6 \pm 3.25}{2}$$

$$x_1 = 4.925$$

$$x_2 = 1.675$$

proof: $(x_1)\ (x_2)/x_1 + x_2$ = focal length

$$\frac{(4.925)\ (1.675)}{6.6} = 1.25$$

The lens is positioned as shown in Figure 16. Magnification of the lens, R, equals the ratio of x_1 to x_2

$$R = x_2/x_1 = \frac{1.675}{4.925} = 0.340$$

Aperture size = (R) (target size)

= (0.340) (0.200)

$\cong$ 0.070 inch

Aperture sensors typically examine a larger area (0.4 inch) but without benefit of the light-gathering ability of a lens sensor. Consequently, the signal available from an aperture sensor is usually much lower. In this design it was necessary to avoid "seeing" the nozzle vanes, but to gather as much signal as possible due to the distance of the target. The most practical approach is to graphically lay out the dimensions involved and evolve the design with successive approximations. The aperture sensor is shown in Figure 17.

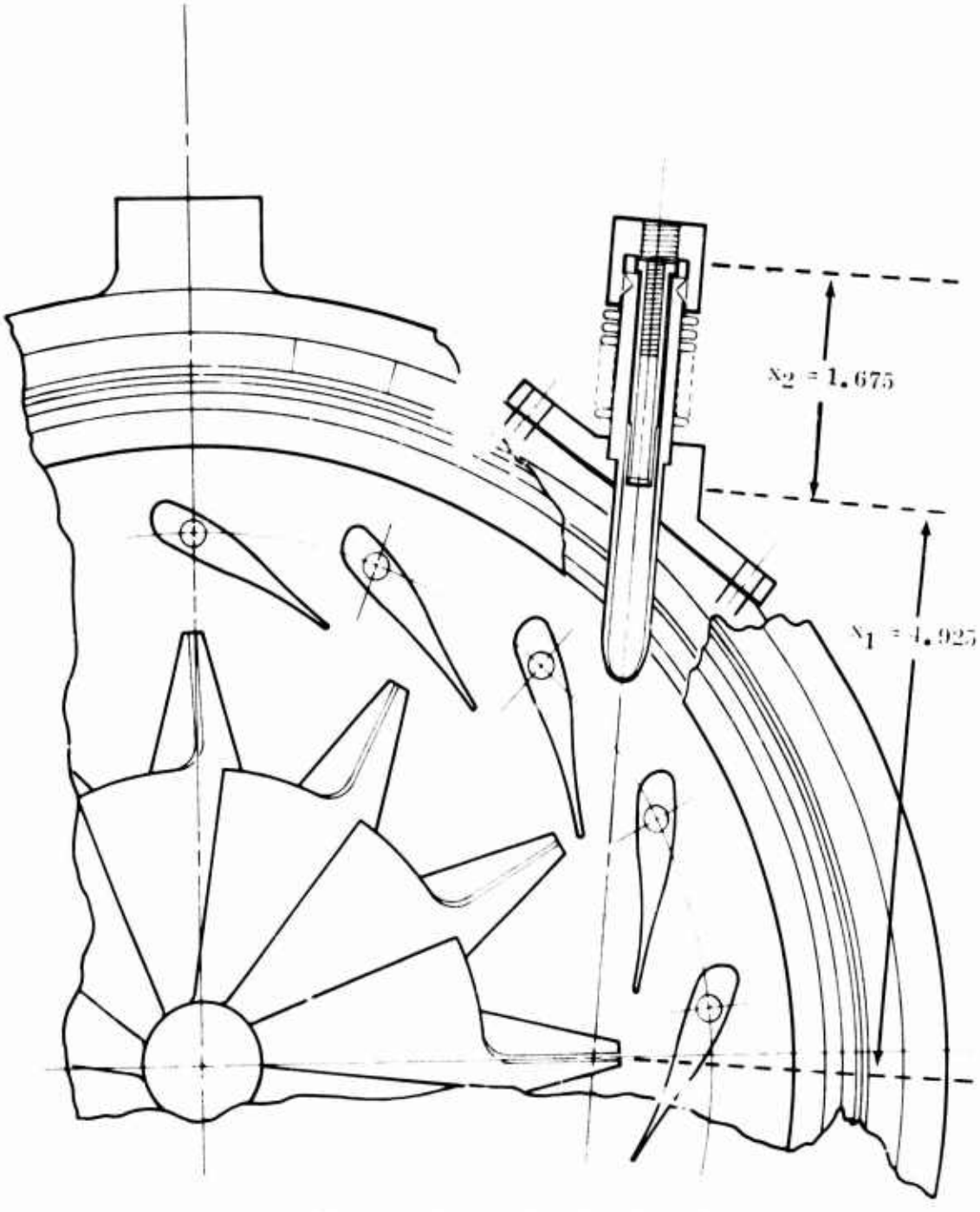

Figure 16. T62T-32 Cross-Section Showing Lens Sensor Installation.

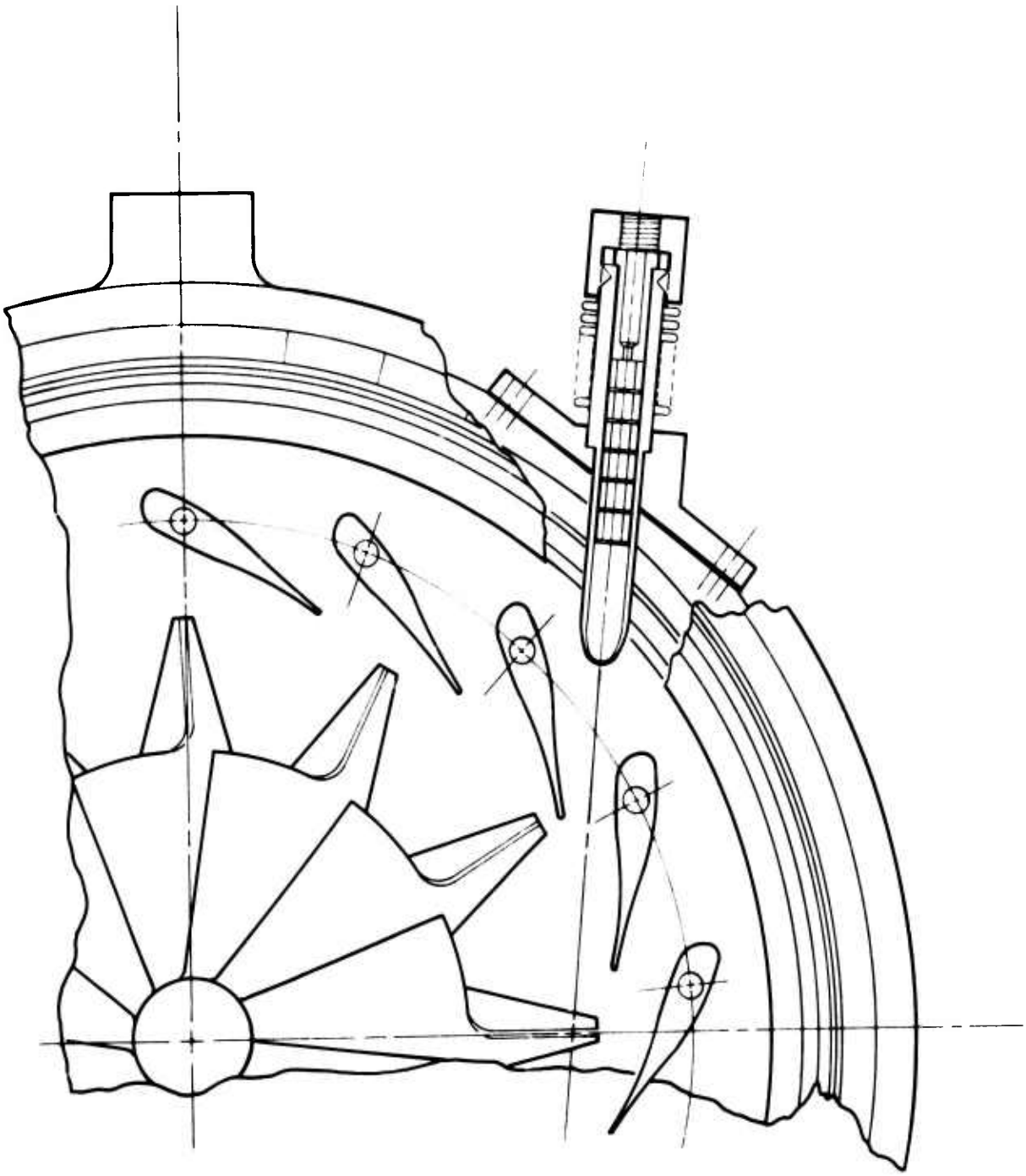

Figure 17. T62T-32 Cross-Section Showing Aperture Sensor Installation.

The T32 probe fixed the distance between the target and the image onto the fiber-optic bundle. The aperture sensor basically functions like a pinhole camera.

The stator sensor views two separate vanes of the nozzle. The area of interest is the leading edge of one vane and the trailing edge of the other. This is shown in Figure 18. The stator sensor design is derived partly from graphical methods and partly through calculation. The first step is to graphically determine the total target area to be viewed and the distance from the target to the lens. These values are 0.910 inch and 1.75 inch, respectively. By preliminary layout it is determined that the image circle (diameter behind lens) is 0.171 inch. With these values a lens-to-aperture distance calculation is made:

$$\frac{\text{distance image to lens}}{\text{distance target to lens}} = \frac{\text{image diameter}}{\text{target diameter}}$$

$$di = \frac{1.75 \times 0.171}{0.910} = 0.329 \text{ inch}$$

A calculation of the lens focal length is now made according to the formula

$$f = \frac{x_1 \; x_2}{x_1 + x_2}$$

$$= \frac{(0.329)\,(1.75)}{2.079} = 0.277 \text{ inch } (7.03 \text{ mm})$$

Next, target areas and aperture sizes are arrived at by successive approximations.

Assume target sizes of 0.2 inch and 0.3 inch. A calculation is then made for aperture size:

$$\frac{\text{distance image to lens}}{\text{distance target to lens}} = \frac{\text{aperture size}}{\text{target size}}$$

$$a_1 = \frac{(0.2)\,(0.329)}{1.75} = 0.0376$$

$$= 0.038 \quad \text{a standard hole size}$$

$$a_2 = \frac{(0.3)\,(0.329}{1.75} = 0.0564$$

$$= 0.052 \quad \text{a standard hole size}$$

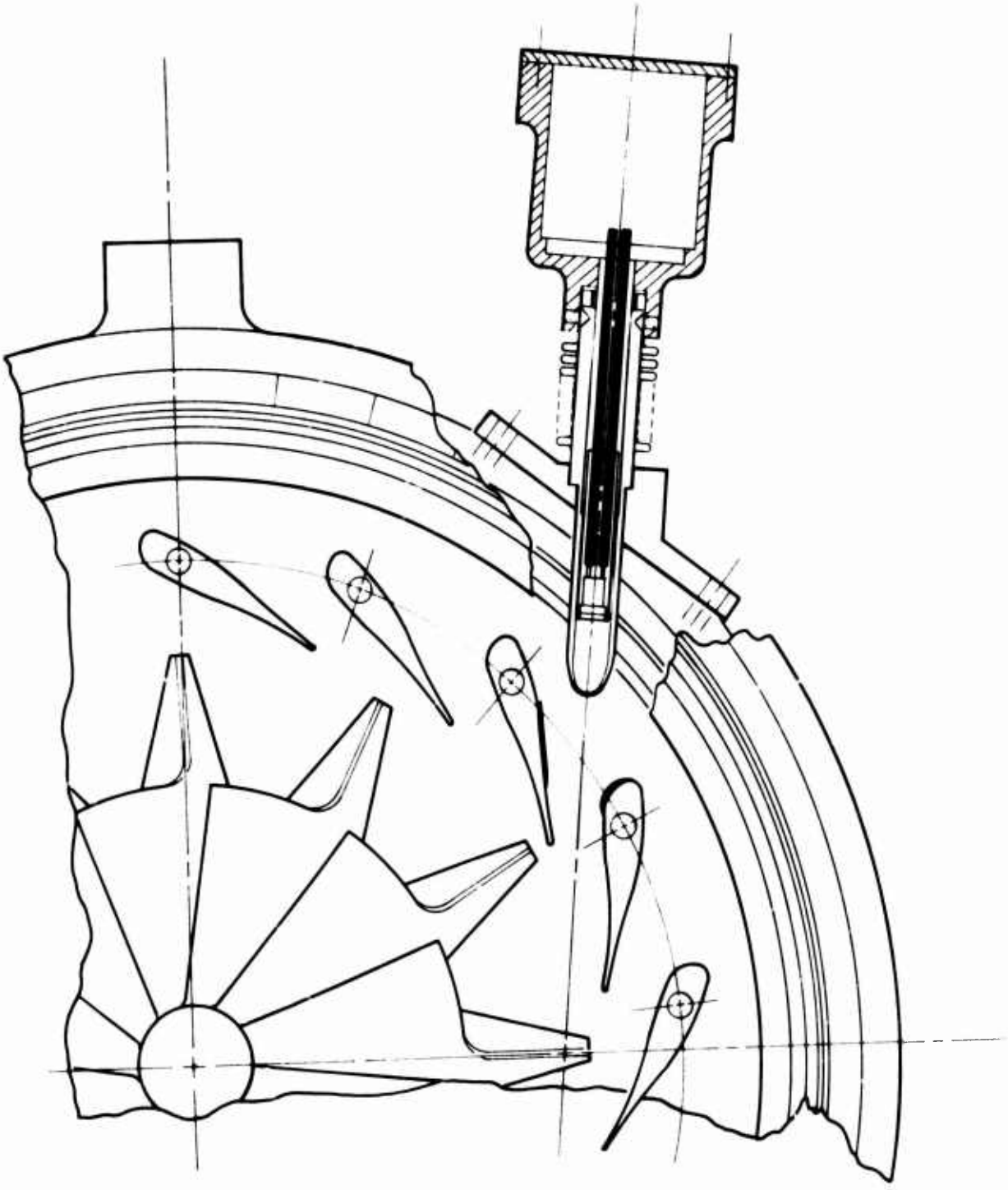

Figure 18. T62T-32 Cross-Section Showing Stator Sensor Installation. (Areas on nozzles viewed by pyrometer are darkened.)

By factoring backwards, we determine the actual target size:

$$T_1 = \frac{(0.038)\ (1.75)}{0.329} = 0.202 \text{ inch}$$

$$T_2 = \frac{(0.052)\ (1.75)}{0.329} = 0.277 \text{ inch}$$

ENGINE TEST AND ANALYSIS

Table IV shows the results of engine testing of the lens, aperture and stator sensors. Figures 19 and 20 are photographs of an oscilloscope trace displaying the output of the lens sensor. Figure 21 shows the output of the aperture sensor. Figure 22 shows one amplifier output of the stator sensor. The mode output of the signal conditioner shown in these figures is a negative signal.

After internal discussions centering on the data of Table IV, the concensus is that the data are representative of the actual metal temperatures. Figure 23, a curve of a T62T-27 (similar to T62T-32), shows that for an ambient condition of 87° F and an output power of 130 hp, the turbine inlet temperature is very close to 1600° F. Generally, the turbine wheel metal temperature under such conditions is 150° F below the turbine inlet temperature.

By necessity, the range of examination during the engine test was limited by an exhaust gas temperature of 1100° F. This EGT limit is the maximum allowable for steady-state conditions to achieve data stabilization. Short excursions to EGT's of 1300° F were conducted and data recorded. These data were transitional and approximate only.

TABLE IV. T62T-32 ENGINE TEST DATA

Sensor Type	Data Point No.	Compressor Inlet Temperature (° F)	EGT Temp. (° F)	Compressor Discharge Pressure (psi)	Fuel Flow (lb/hr)	Power Output (hp)	Speed (kHz)	Pyrometer Output Channel A			Pyrometer Output Channel B		
								Avg. (° F)	Avg. Peak (° F)	Max. Peak (° F)	Avg. (° F)	Avg. Peak (° F)	Max. Peak (° F)
Lens	14	87	1130	42.7	122.0	131.0	1995	1462	1471	1468			
	15	87	1064	42.7	115.5	121.4	2002	1403	1408	1406			
	16	87	1002	42.7	108.8	110.1	2008	1346	1346	1351			
	17	88	959	42.7	103.5	100.8	2013	1306	1306	1309			
	18	88	915	42.7	97.2	90.1	2017	1247	1247	1253			
	19	88	839	42.0	86.6	70.5	2024	1144	1145	1158			
Stator	20	84	1125	42.7	121.5	130.7	1995	1564	1563	1565	1567	1568	1569
	21	88	1071	42.7	115.5	121.0	1999	1518	1519	1522	1514	1514	1515
	22	88	1008	42.5	109.0	110.6	2005	1464	1466	1472	1463	1464	1465
	23	88	955	42.9	103.5	100.8	2012	1427	1427	1434	1423	1423	1426
	24	89	911	42.7	97.5	90.1	2015	1390	1390	1398	1382	1382	1387
	25	91	876	42.5	92.3	81.0	2020	1360	1362	1369	1346	1348	1352
Aperture	26	90	1146	42.7	121.5	130.1	1993				1350	1391	1436
	27	90	1078	42.7	115.0	120.2	2001				1233	1302	1370
	28	90	1023	42.7	109.0	110.8	2008				1116	1220	1340

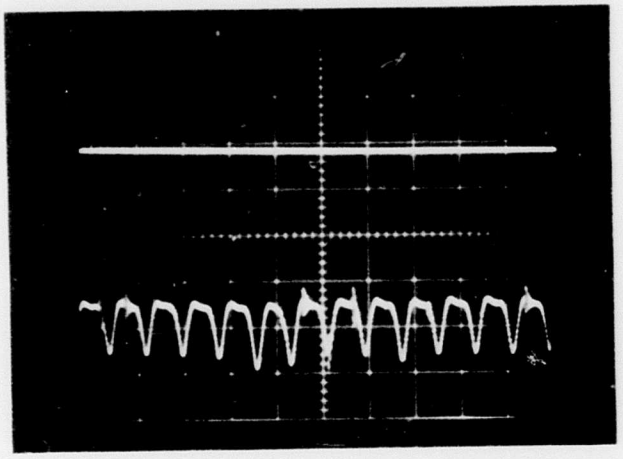

Horizontal 100 μ sec/div Vertical 20 mV/div

Figure 19. Lens Sensor Trace Photo at 1702° F Indicated Turbine Wheel Temperature.

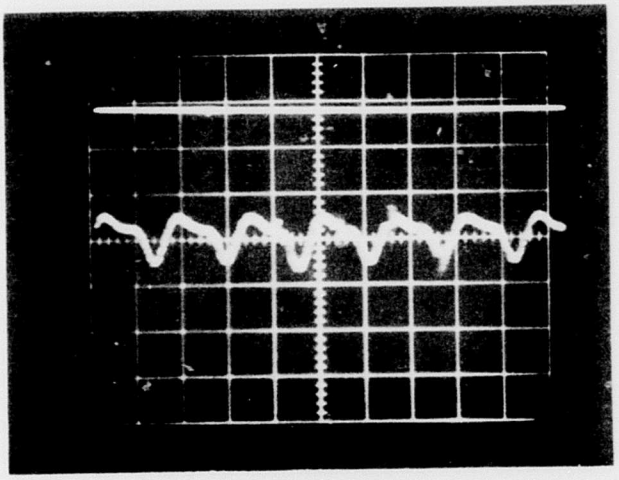

Horizontal 50 μ sec/div Vertical 5 mV/div

Figure 20. Lens Sensor Trace Photo at 1458° F Indicated Turbine Wheel Temperature.

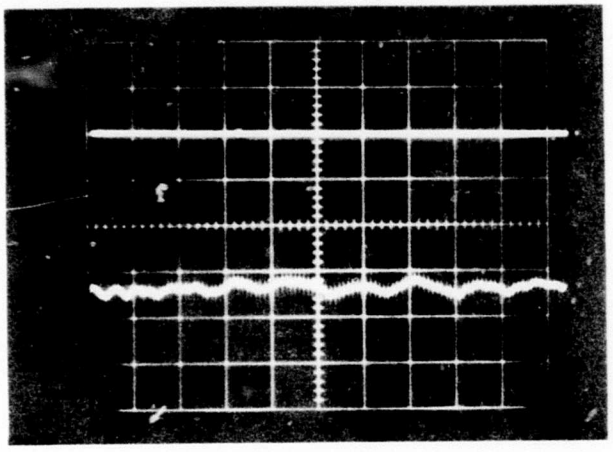

Horizontal 5 μ sec/div Vertical 10 mV/div

Figure 21. Aperture Sensor Trace Photo at 1340° F Indicated Turbine Wheel Temperature.

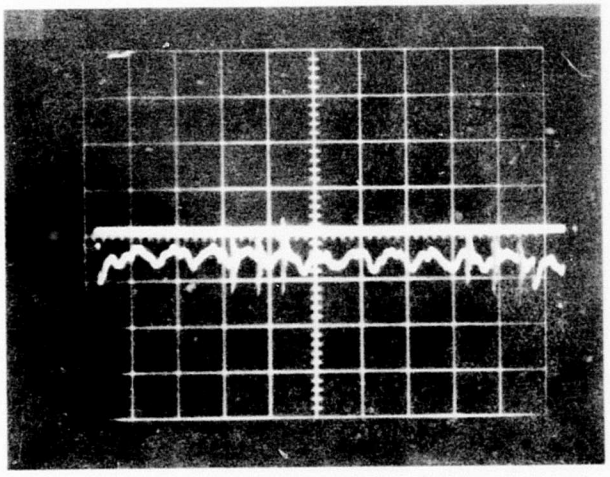

Horizontal 100 μ sec/div Vertical 10 mV/div

Figure 22. Stator Sensor Trace Photo at 1568° F Indicated Nozzle Vane Temperature.

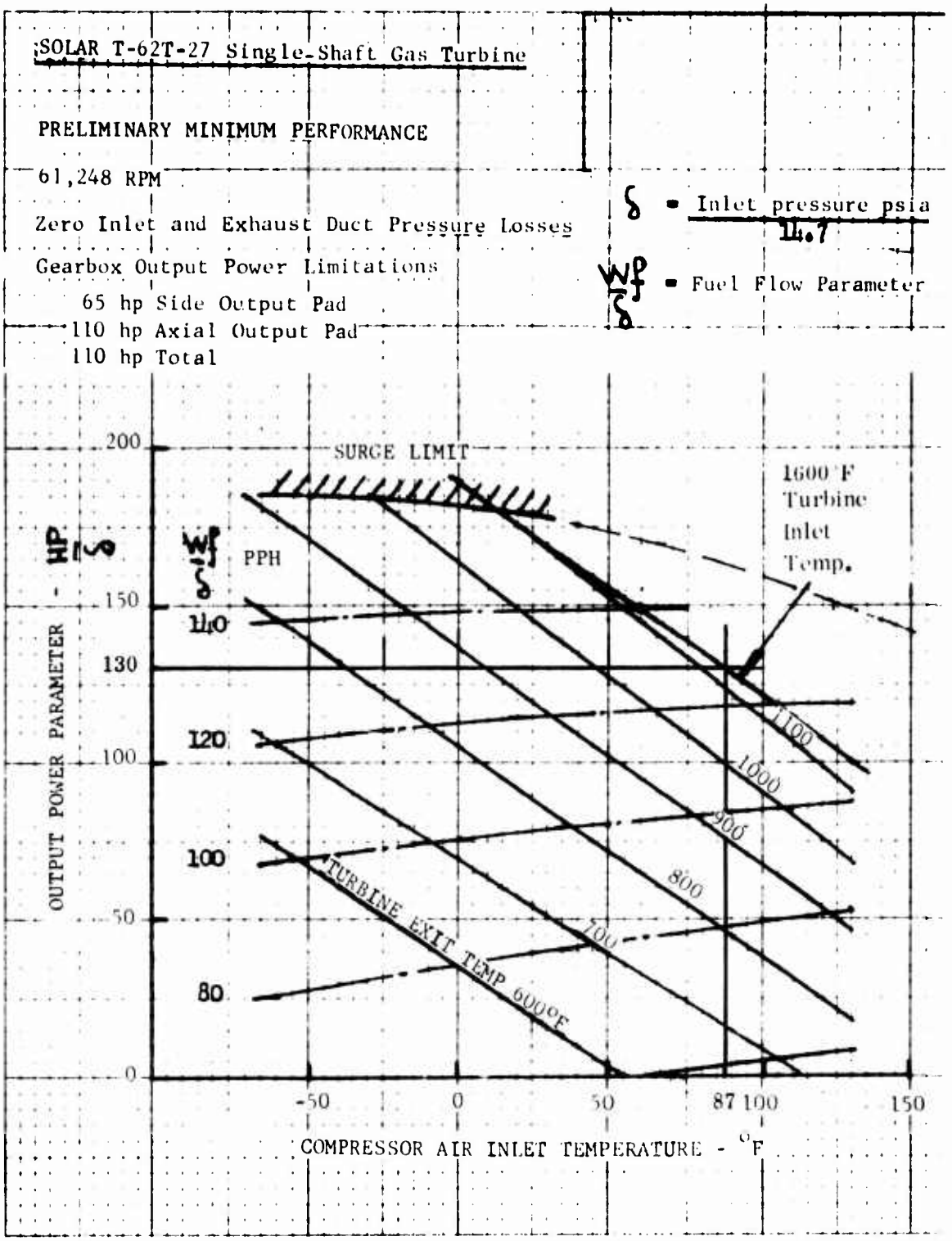

Figure 23. Solar T62T-27 Single-Shaft Gas Turbine Performance Curve.

Table V shows comparisons of engine test data pyrometer instrument readings to theoretical turbine inlet temperatures. The column marked ΔT indicates the magnitude and direction that the pyrometer readings differ from theoretical values.

TABLE V. COMPARISONS OF ENGINE TEST DATA PYROMETER READINGS TO THEORETICAL TURBINE INLET TEMPERATURES

Data Point		Pyrometer Average Mode (° F)		Computer Program Theoretical (° F)	ΔT(° F)
14		1462		1442	+20
15		1403	Target:	1362	+41
16	Lens	1346	Turbine	1284	+62
17	Sensor	1306	Wheel	1225	+81
18		1247		1166	+81
19		1144		1065	+79
20		1563		1590	-27
21		1519	Target:	1507	+12
22	Stator	1466	Nozzle	1434	+32
23	Sensor	1427	Vanes	1374	+53
24		1390		1317	+73
25		1362		1264	+98
26		1350	Target:	1446	-96
27	Aperture	1233	Turbine	1364	-131
28	Sensor	1116	Wheel	1296	-180

Assumptions:

(1) Metal temperature of turbine wheel is approximately 150° F below turbine inlet gas temperature under operating conditions. This is analytically derived and not a measured difference.

(2) Metal temperature of stator or nozzle vanes is approximately equal to gas temperature under operating conditions.

The theoretical values were obtained by a computer program, into which the data obtained from the engine test were inserted. The data used were ambient temperature, engine speed, engine load, exhaust gas temperature and compressor discharge pressure.

The probe inserted into the T62T-32 air inlet housing used a small 0.040-inch purge hole for lens cleaning. This method proved to be only moderately successful in the case of aperture and stator sensors. These sensors were soot-coated after very short operating intervals. The lens sensor emerged considerably cleaner after a similar short operating interval. Total engine operating time consumed in testing was 3.8 hours.

Figure 24 is a strip chart recording displaying the relationship between exhaust gas temperature and the processed pyrometer signal after detection, amplification and linearization. The chart reads from right to left and consists of three slow manual cycles of no load to full load followed by three rapid cycles of load dumping with engine shutdown. As seen from the recording, there is very close tracking between the two methods.

Figure 25 shows the T62T-32 Titan engine mounted on a test stand with a sensor probe mounted into the air inlet housing. Figure 26 shows the engine water brake dynamometer loading system and engine instrumentation.

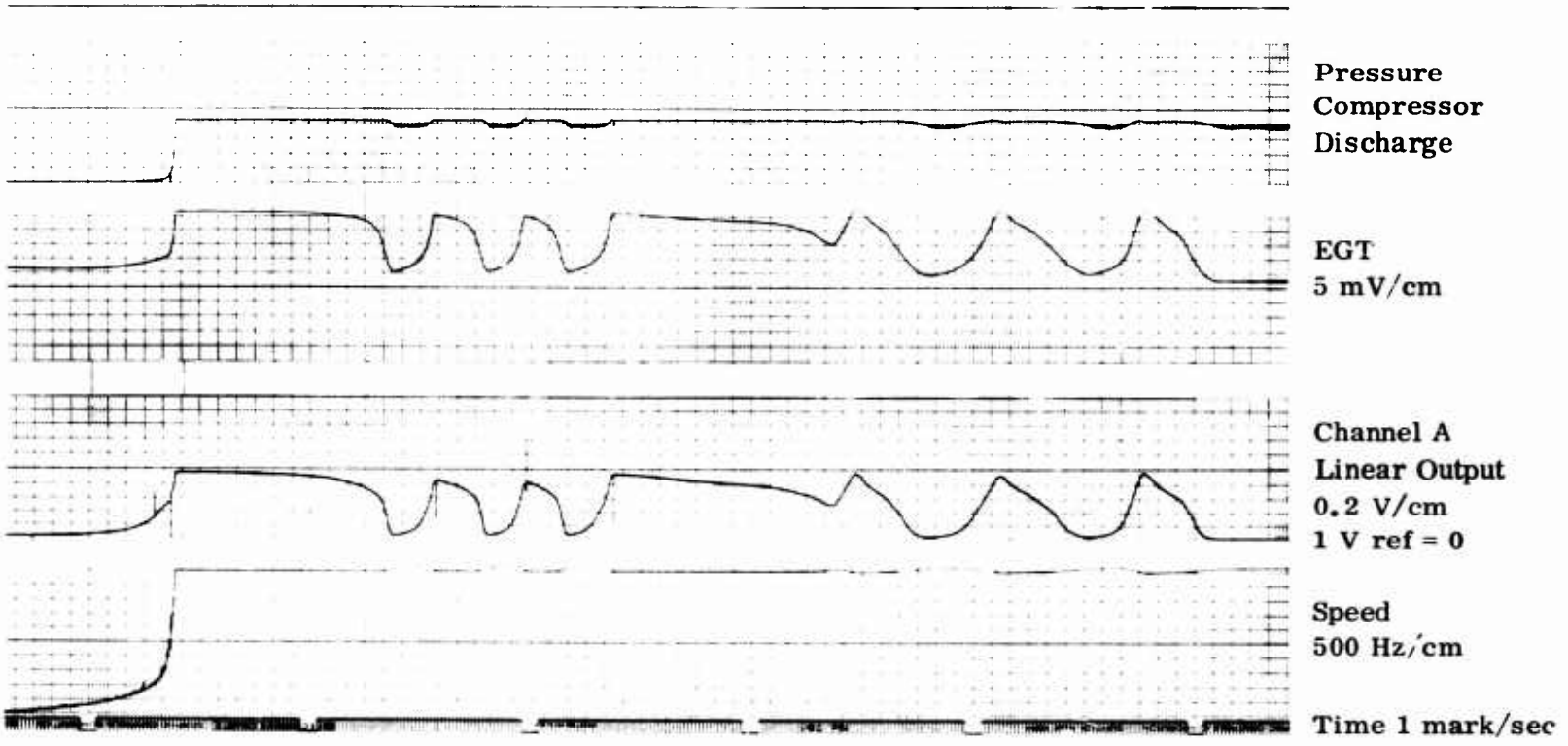

Figure 24. Strip Chart Recording Showing Comparison Between Pyrometer Readout and Exhaust Gas Temperature.

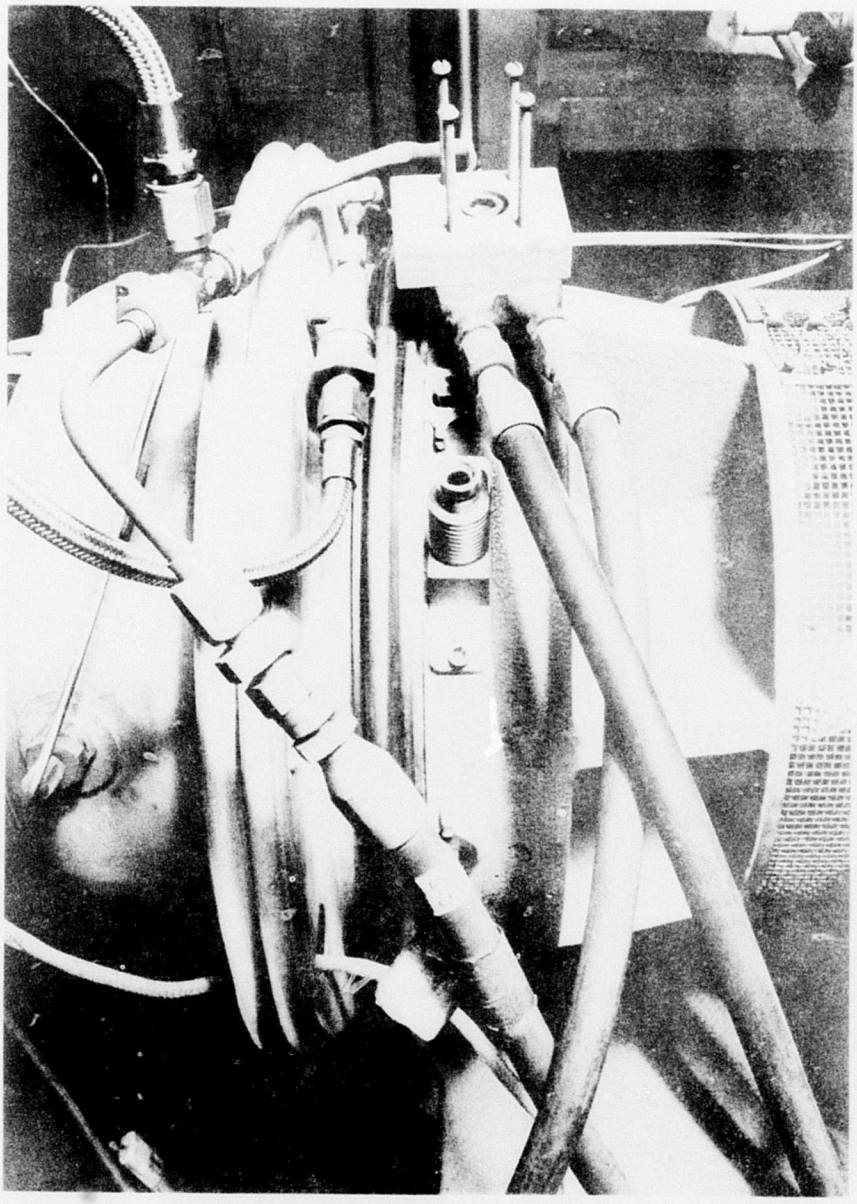

Figure 25. Solar T62T-32 Showing Sensor Probe Inserted Into Air Inlet Housing.

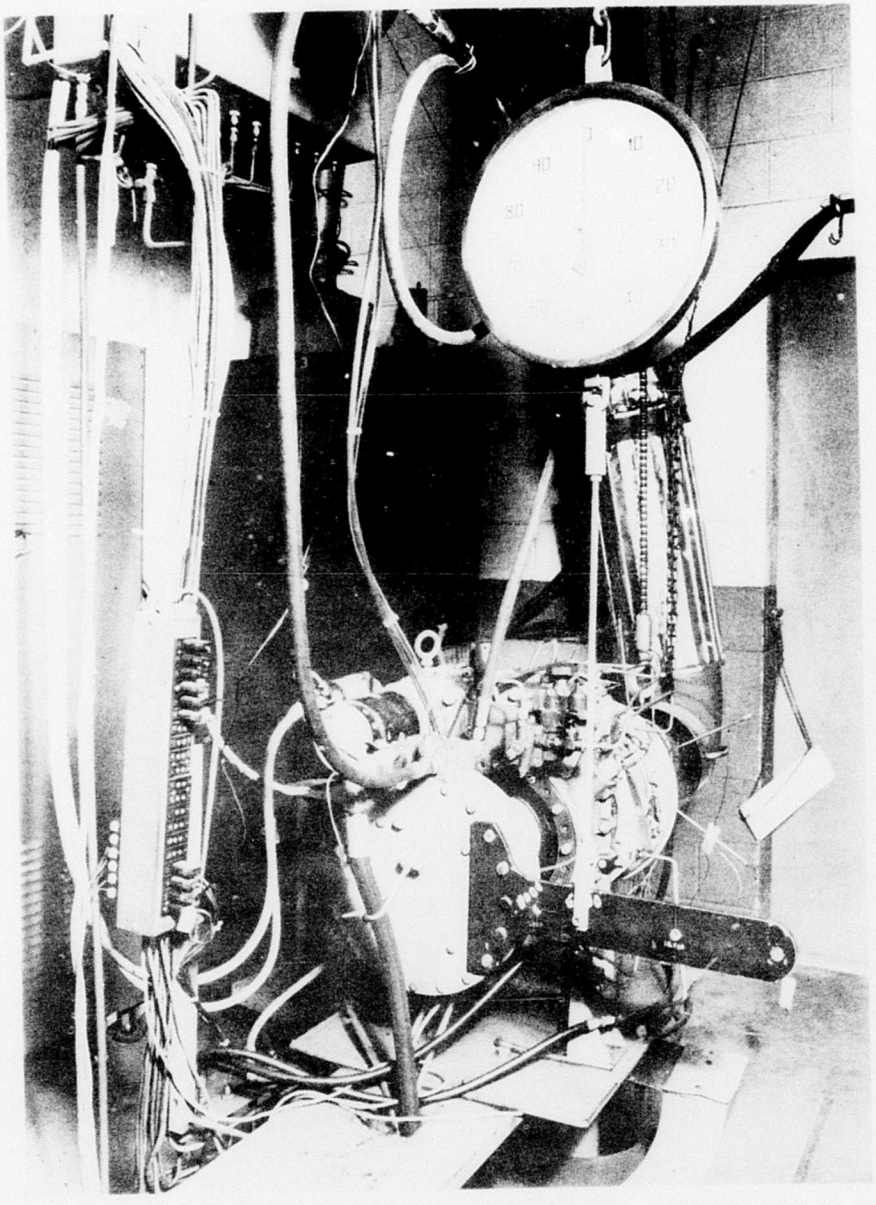

Figure 26. Solar T62T-32 Titan Engine Mounted on Test Stand and Instrumented.

CONCLUSIONS

A turbine blade temperature measuring system was designed and tested to measure the turbine wheel temperatures of a small gas turbine engine. The laboratory and engine tests demonstrated that radiation pyrometry techniques are capable of adapting to a small gas turbine engine and exhibiting signals proportional to temperatures that appear to be reasonably accurate.

Small turbine engines characteristically increase the difficulty of probe adaptation and signal processing. The highly nonlinear detector output signal diminishes by a factor of 10 for each 200° F downward extension of range. The signal available for processing becomes exceedingly small, so small in fact that device limitations contribute significant error.

Frequency response of 50 kHz was attained by shifting the bulk of necessary gain into the linearizer design to use the full gain bandwidth product of the preamplifier. Major performance improvements can be realized by using better devices in the preamplifier stages as they become available. The optical conversion to an electrical signal is the key area for performance improvements.

A possible approach for future study would be to use an optical-to-frequency conversion technique with signal processing done similar to frequency modulation methods. If changes of frequency in response to changes of radiation were highly predictable and repeatable, significant advantage could be taken of digital processing methods. Potential advantages of this technique are reduced electrical noise problems in transmission from engine to signal processor, digital processing for linearization improving accuracy, and reduced cost in production.

The closer any turbine engine is operated to its design limits, the greater the necessity for radiation pyrometry. As a measuring instrument used in engine development, radiation pyrometry, as configured presently, has limitations toward the low end of its measuring range. As a control element or protection monitor, radiation pyrometry becomes potentially very attractive due largely to accuracy at high signal levels.

Engine testing is providing the necessary confidence toward acceptance of radiation pyrometry for use with gas turbine engines.

LITERATURE CITED

1. Duffy, T. E., et al, "Research Analysis of Advanced Sensors for Turbine Inlet Gas Temperature", conducted by Solar Division of International Harvester Company, San Diego, California, under Naval Air Systems Command Contract N00019-69-C-0574 (June 1969 to July 1970).

2. Forsyth, W. E., "Optical Pyrometry", Temperature, Its Measurement and Control in Science and Industry, New York: Reinhold Publishing Co., 1941 , pp. 1115.

3. Barber, R., and Land, T., "The Place of Photo Voltaic Detectors in Industrial Pyrometry", Temperature, Its Measurement and Control in Science and Industry, Part II, New York: Reinhold Publishing Co., 1962 , pp. 391.

4. Jones, R. Clark, "Phenomenological Description of the Response and Detecting Ability of Radiation Detectors", Proceedings of the IRE, Sept. 1959, pp. 1495-1502.

LIST OF SYMBOLS

C_1	constant = 3.7412×10^{-12} w-cm^2
C_2	constant = 1.438 cm - °K
D	distance from objective lens to target
F	optical transfer factor
F_c	transfer factor
N total	total radiance at all wavelengths
$N_{b\lambda}$	radiance (radiant power) from a blackbody emitted at a wavelength, λ
n	temperature exponent
R_λ	responsivity of a detector
S	detector signal (current)
T	temperature of a solid body
ϵ	emittance
ϵ_c	emittance value present during calibration
ϵ_λ	emittance at wavelength, λ
$\epsilon_{0-\infty}$	total emittance
λ	wavelength (cm)
λ_{max}	wavelength at which the maximum radiance is emitted
σ	Stefan-Boltzmann constant
ϕ	radiant power arriving at the detector